

4-2014

Design of a Portable Fast Scan Cyclic Voltammetry System for Measuring Neurotransmitter Levels

Jayson Foster
Grand Valley State University

Follow this and additional works at: <https://scholarworks.gvsu.edu/theses>



Part of the [Engineering Commons](#)

ScholarWorks Citation

Foster, Jayson, "Design of a Portable Fast Scan Cyclic Voltammetry System for Measuring Neurotransmitter Levels" (2014). *Masters Theses*. 713.
<https://scholarworks.gvsu.edu/theses/713>

This Thesis is brought to you for free and open access by the Graduate Research and Creative Practice at ScholarWorks@GVSU. It has been accepted for inclusion in Masters Theses by an authorized administrator of ScholarWorks@GVSU. For more information, please contact scholarworks@gvsu.edu.

Design of a Portable Fast Scan Cyclic Voltammetry System for Measuring
Neurotransmitter Levels

Jayson Foster

A Thesis Submitted to the Graduate Faculty of

GRAND VALLEY STATE UNIVERSITY

In

Partial Fulfillment of the Requirements

For the Degree of

Master of Science in Engineering

Padnos College of Engineering

April 2014

Acknowledgments

Dr. Eric Ramsson, Dr. Samhita Rhodes, Chris Dickson, and Jeremy Pace for the work on the design and theory behind the project and the NIH R15 Academic Research Enhancement Award along with a grant from the NSF for funding.

Abstract

The goal of this project is to design, build, and validate a more economic portable Fast Scan Cyclic Voltammetry (FSCV) device to measure the concentration of neurotransmitters like dopamine. The device will allow educational demonstrations in classrooms and allow researchers to gather data without the financial burden of a full cost system. The device is created on a Printed Circuit Board (PCB) that interfaces with a standard computer through MATLAB. This allows data collected on the PCB to be accessible to the user to display and analyze at will, all while maintaining the system's portability and low cost. The device was tested using a dummy cell and artificial cerebral spinal fluid (ACSF), comparing the results to those obtained from the gold standard laboratory equipment for the same simulated experimental setup. Our device is able to show the main features that distinguish a voltammogram of the dummy cell and dopamine. Priced at about \$200, which is \$8,800 less than the gold standard equipment, our device demonstrates the feasibility of a useful low cost.

Table of Contents

1. INTRODUCTION	7
2. LITERATURE REVIEW	9
2.1. PHYSIOLOGY	9
2.1.1. NEURONS AND NEUROTRANSMITTERS	9
2.1.2. DOPAMINE.....	11
2.2. DESIGN.....	12
2.2.1. TECHNIQUES TO MEASURE NEUROTRANSMITTERS	12
2.2.2. EXISTING DEVICES.....	17
3. SPECIFIC AIMS	19
4. METHODOLOGY	20
5. RESULTS	25
6. DISCUSSION.....	31
7. FUTURE WORK	35
8. CONCLUSION	36
BIBLIOGRAPHY.....	37
APPENDIX I – COMPONENT DATA SHEETS.....	39
APPENDIX II – SCHEMATIC	61
APPENDIX III – MATLAB CODE	66
APPENDIX IV – DAC MICROCONTROLLER CODE.....	72
APPENDIX V – ADC MICROCONTROLLER CODE.....	75

Table of Figures and Tables

Figure 1: Anatomy of a nerve cell (National Institutes of Health)	10
Figure 3: Push-pull method used by (Kottegoda, Shaik, & Shippy, 2002)	14
Figure 4: Microdialysis method visual courtesy of (Syslová, et al., 2012)	15
Figure 5: Voltammetry (UCLA Department of Psychology)	16
Figure 7: Cheapstat potentiostat developed by (University of California, Santa Barbara, 2011)	18
Figure 6: NI PCI-6711 High-Speed Analog Output card (left) and NI PCI-6052E High-Speed Analog Input card (right).	18
Figure 8: Functional Block diagram for hardware design	21
Figure 9: DAC Amplifier Design	22
Figure 10: Current to Voltage Conversion and Amplification	22
Figure 11: Functional block diagram for software	23
Figure 12: Device output - voltammetry stimulation waveform	26
Figure 13: Raw data from ADC (left) and filtered data (right).....	27
Figure 14: Result from device with dummy cell (left) compared to Gold Standard system dummy cell (right).....	27
Figure 15: Background Current of the Electrode Measurements with Device	29
Figure 16: Gold Standard Equipment Background Current Measurement.....	29
Figure 17: Dopamine Measurements taken with the device	30
Table 1: Dopamine Current Peak Measurements	31

1. Introduction

Neuroscience research is critical to our understanding of how the brain works; however, this research is very complex due to the small signals and intricate cellular networks involved. While information transfer within neurons is transmitted via action potentials, neurons communicate with each other using neurotransmitters that chemically communicate information from one neuron to another. Neurotransmitter dysfunctions have been found to play a significant role in diseases such as schizophrenia (Davis, Kahn, & al, 1991), Parkinson's (Hisahara & Shimohama, 2011), and attention deficit/hyperactivity disorder (del Campo, Chamberlain, Sahakian, & Robbins, 2011). In order to study these networks, research methods such as Fast-Scan Cyclic Voltammetry (FSCV) are used to measure the changes in neurotransmitters and understand their neural function.

Current FSCV systems are cost-prohibitive, requiring researchers interested in studying neurotransmitter release to incur a large capital outlay. The development of a portable, cost-effective FSCV device capable of measuring neurotransmitter concentrations during laboratory or classroom experiments would allow students to develop a deeper understanding of neuroscience. Increasing the availability of low cost FSCV devices will allow smaller, teaching-focused, and financially-restricted institutions to enhance their pedagogy by exposing their students to cutting edge neurobiology techniques. In addition, these devices will allow faculty at such institutions to set up modest research laboratories and gather preliminary grant data. Thus, a more budget friendly FSCV device will enable broader academic pursuits at both the graduate and undergraduate levels.

FSCV uses probes that are thinner than a human hair to minimize damage to the tissue, and a data collection system capable of recording up to 1000 data points per second. Currently, our laboratory uses the gold standard system comprised of a desktop computer containing two PCI slots, two data acquisitions cards, and a Chem-Clamp potentiostat. This system is widely used in the field, however it can cost in the range of \$8,000-10,000.

The proposed project is a self-contained, low-cost, USB powered FSCV device designed to be portable and adaptable. The device will be capable of generating the necessary voltage required to produce voltammetry effects, evoking NT release with electrical stimulation, and measuring the resultant change in current in the electrode. The device will utilize the same electrodes as those used with the current gold standard equipment, allowing established labs to continue using and producing these electrodes that cost about 15 cents each. In order to achieve these capabilities, it will require the design and integration of customized hardware and software systems; most notably for data acquisition and for signal generation.

With the design and implementation of an economical and portable system for FSCV, the door will be opened to many research institutions and students allowing for the measurement of neurotransmitters without spending up to \$10,000 for the ‘gold standard’ in FSCV equipment. This will allow the possibility of introducing the technique into the classroom to demonstrate the transmission of neurotransmitters where previously only theory and textbooks could be used to study these processes.

2. Literature Review

2.1. Physiology

2.1.1. Neurons and Neurotransmitters

The nervous system is the control system of the human body and the most complex computational system in existence. It is able to perform a large number of calculations very fast, receive and sift through a vast array of sensory input and control the muscular system of the body. While most of the anatomy of the nervous system is well understood, the brain's complexity makes it difficult to understand. Therefore, to help understand this complex organ better, it would be beneficial to track neuronal activity and determine the parts of the brain that are active during certain events.

The functionality of a neuron is best described by studying the different regions of a typical cell – these regions consist of the cell body, dendrites, axon, and the synaptic terminals. As it can be seen in Figure 1 below, the cell body (or soma) is the metabolic center of the neuron that holds the nucleus. The dendrites extending from the cell body are the main processes through which the neuron receives input from other nerve cells. Neuronal output is conducted via the axon to other cells. At the end of the axon are many branches that end in presynaptic terminals. These terminals are within close range to other neurons dendrites, either forming a synapse that allows for communication between the different cells or terminating in a target organ or tissue. For example, motor neurons whose axons terminate in the neuromuscular junction and stimulate the muscles for muscle contraction.

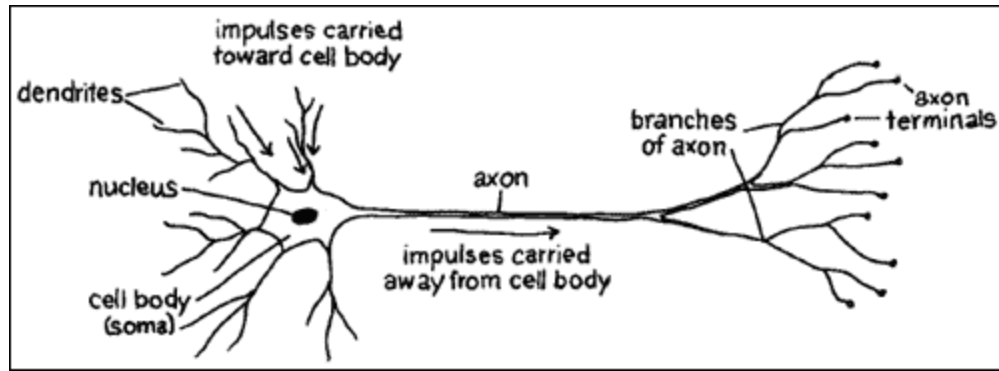


Figure 1: Anatomy of a nerve cell (National Institutes of Health)

After a stimuli is applied to a neuron, the cell has an electrical response that may be local (restricted to the place that received the stimulus) or propagated (may travel through the neuron and its axon). Propagated electrical impulses are called action potentials, which forms the basis for neuronal communication via the synapses. Synapses are not actual physical connections between cells; instead the two cells are separated by a synaptic cleft. This can be seen in detail below in Figure 2, where the interface between the presynaptic neuron and postsynaptic neuron has been shown in detail. In order for the two cells to communicate, chemical signals are used to propagate the action potential present in the presynaptic neuron. The action potential stimulates the release of neurotransmitters when it reaches the synaptic terminals, resulting in an expulsion of neurotransmitter molecules into the synaptic cleft. The neurotransmitters then bind to receptors on the postsynaptic neuron and trigger the opening of ion channels. These channels opening result in a change in local membrane potential, which may or may not create an action potential depending on the size of the change in voltage. In order to clear the receptors and allow for another possible stimulation, after binding to the receptor sites the neurotransmitter molecules may either be degraded by enzymes present in the cleft or be taken back up into the

presynaptic neuron (Waxman, 08/2009). So all neural cell signaling consists of an electrical and chemical component, each of which is important to understand nerve function.

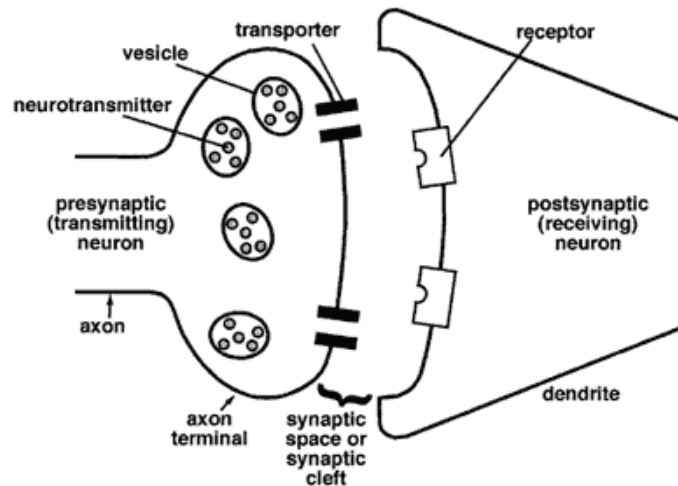


Figure 2: Synapse between two neurons (National Institutes of Health)

There are a great variety of neurotransmitters with over fifty currently identified. Some of the most well-known are acetylcholine, dopamine, serotonin, epinephrine, and glutamate. These all have specialized uses and are released in specific anatomical locations. Acetylcholine, for example, is the primary neurotransmitter for stimulating muscles and transmitting information through the parasympathetic nervous system. Epinephrine is the primary neurotransmitter in the sympathetic nervous system, while dopamine is largely present in the brain as a neurotransmitter for reward-motivated behavior (Chara, 2010).

2.1.2. Dopamine

Dopamine is one of the prominent neurotransmitters in the human body, and depending on the postsynaptic receptor it can produce both excitatory and inhibitory postsynaptic potentials (Helgeson, 2010). For example, in the central nervous system dopamine is involved in control of

mood, movement, cognition, motivation, and reward. Here it produces an excitatory stimulation and the amount of dopamine present is directly related to the generation of the postsynaptic action potential. In contrast, in the peripheral nervous system dopamine acts as a more regulatory hormone controlling Na^+ homeostasis in kidney, renal blood flow, and cardiovascular functions (Syslová, et al., 2012). Here dopamine has an inhibitory role, making it harder for postsynaptic cells to generate action potentials. An example of this is in the blood vessels where it inhibits norepinephrine release which allows the local blood vessels to dilate (Tayebati, Lokhandwala, & Amenta, 2011). Research efforts into dopamine are primarily concentrated on its role in Parkinson's disease, schizophrenia, drug addiction, attention deficit hyperactivity disorder, along with the learning process. Accurately measuring the levels of dopamine released thus becomes important when studying disease mechanisms.

2.2. Design

2.2.1. Techniques to measure neurotransmitters

The earliest techniques to measure neurotransmitter levels required brain tissues extracted post mortem. While post mortem analysis was relatively quick and simple it failed to elaborate on more elusive and detailed information. So while this technique was able to find the amount of neurotransmitters present in the brain, it could do so only at one singular point in time: the moment of demise. This left out necessary dynamic information regarding neurotransmitter levels (Korpi, Kleinman, Goodman, & Wyatt, 1987).

A more modern approach for *in vitro* measurement of neurotransmitter levels involves microdissections instead of whole brain tissue excision and analysis. However, microdissections are unable to provide a necessary level of detail due to the unavoidable delay between tissue

death and final tissue analysis. Neither of the aforementioned techniques are able to measure changes in neurotransmitter levels dynamically in response to the application of stimuli (Chang, Keller, & Sretavan, 2006).

The two main historic methods of *in vivo* measurement of neurotransmitters included the use of a cortical cup or utilizing the push-pull technique. The cortical cup could measure neurotransmitters released from the surface of the brain, as it was attached directly to the cortex. The cup itself was filled with a perfusion fluid such as artificial cerebrospinal fluid, attached to the brain with a silicone gel and held in place with dental cement. The neurotransmitters then diffused into the perfusion fluid in the cup, whereupon the cup could be removed and the fluid analyzed. The main purpose of this technique was to monitor amino acids and acetylcholine, but this method had a number of flaws. It could not be performed on conscious animals, and since the technique relied upon diffusion it could not measure concentrations deep within the brain tissue (Mitchell, 1963) (Moroni & Pepeu, 1984).

On the other hand, the push-pull technique was able to measure neurotransmitter concentrations deeper in the brain, and the set up can be seen below in Figure 3. This rather simple technique involved two tubes implanted into the brain – one pushing perfusion fluid into the tissue while the other pulled the fluid back out. As the fluid came into contact with the deep brain tissue, neurotransmitters were swept into the flow and therefore could be analyzed. The main drawback of this technique was the damage caused to the tissue by tubal implantation (Kottegoda, Shaik, & Shippy, 2002).

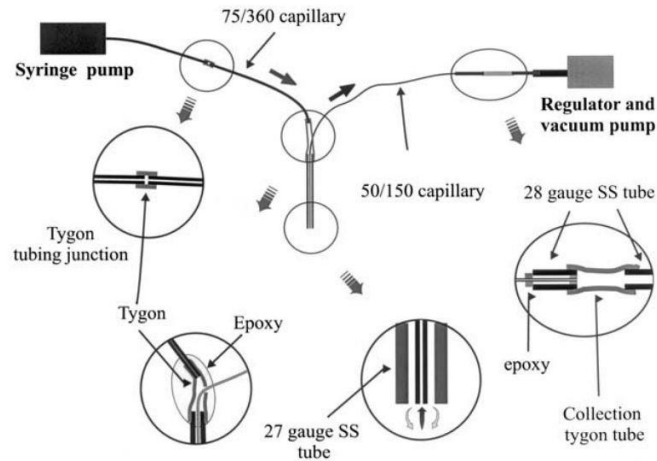


Figure 3: Push-pull method used by (Kottegoda, Shaik, & Shippy, 2002)

Current techniques for measurement of neurotransmitter concentrations *in vivo* include the microdialysis technique and voltammetry. The microdialysis technique operates in much the same way as the push-pull method as it relies on diffusion to collect neurotransmitters for measurement. However, instead of tubes, a light dialysis membrane is used – as seen below in Figure 4 – which minimizes tissue damage during surgery. After the membrane is implanted into the region of the brain that is being monitored, perfusion fluid is pumped near the membrane. The neurotransmitters present in the extracellular fluid of the brain then collect in the perfusion fluid as a result of passive diffusion while special filters keep out the larger unwanted molecules such as enzymes. The usefulness of microdialysis is its ability to selectively monitor the extracellular environment for extended periods of time in both anesthetized and awake animals, along with providing more information about neuronal activity and metabolism than post-mortem methods (Muller, 2002).

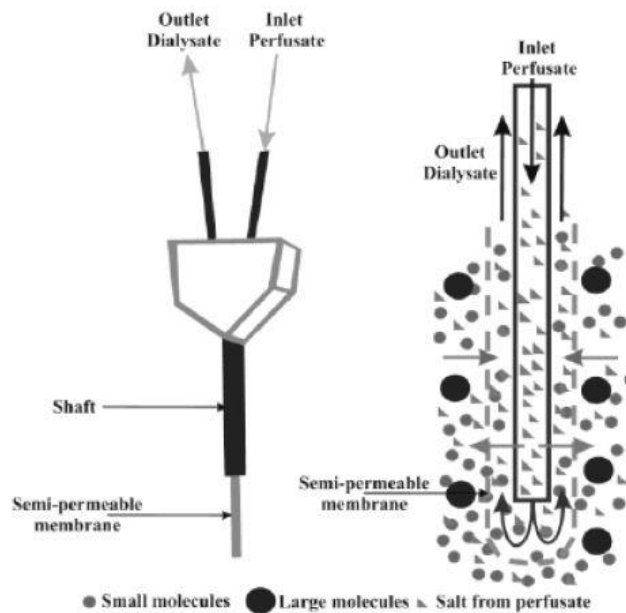


Figure 4: Microdialysis method visual courtesy of (Syslová, et al., 2012)

Finally, *in vivo* voltammetry is the second method capable of directly monitoring neurotransmitters in real-time. While there is contention between voltammetry and microdialysis experts regarding which one is the better technique (Jones, Gainetdinov, & Marc, 1999), and both certainly have their strengths; it can be argued that voltammetry is superior as it uses smaller electrodes cause less tissue damage (Jaquins-Gerstl & Michael, 2009) and allows recordings from freely moving animals (Garrus, Kilpatrick, Bunin, Michael, & al, 1999). Voltammetry is performed by holding the working electrode at a potential at which the neurotransmitter cannot oxidize – for example, if measuring dopamine the electrode is held at -0.4 V. As shown in Figure 5, the potential of the working electrode is then ramped up linearly to an oxidizing potential (in the case of dopamine 0.6 V, but to enhance the sensitivity of the reading, the voltage goes up to 1.3V) and then back down to the resting potential at a scan rate of

400 V/s ten times per second. When the targeted neurotransmitter, in our example dopamine, is present in the solution, it is oxidized during the positive voltage sweep to form dopamine-o-quinone and then reduced back to dopamine during the negative voltage sweep. The redox reactions taking place cause electrons to transfer between the molecules and the working electrode creating a current that is measurable. As this transfer of electrons is directly proportional to the amount of molecules of dopamine present, this method allows for an accurate reading of the amount of dopamine present in a small time window.

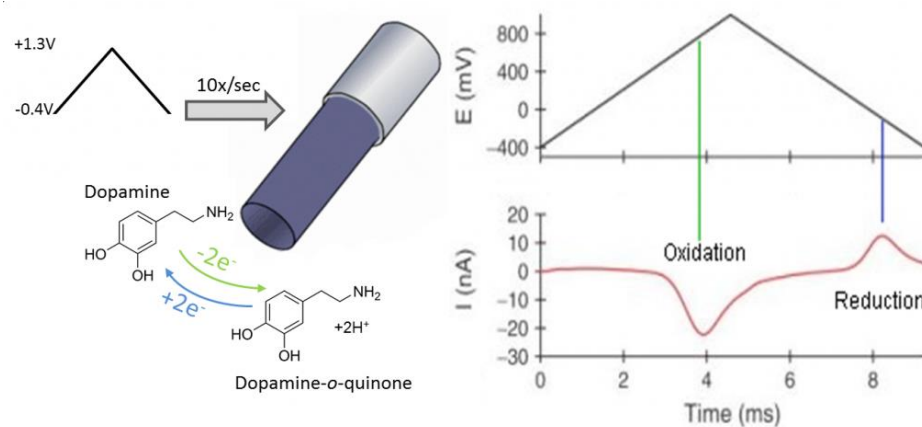


Figure 5: Voltammetry (UCLA Department of Psychology)

Current *in vivo* techniques like microdialysis and voltammetry still require surgical implementation of either a probe or electrodes; however they are preferable to the alternative of post mortem static analysis or the tissue damaging push-pull method. The techniques themselves also give much higher temporal and local resolution, which make microdialysis and voltammetry much more desirable techniques.

The microdialysis technique uses sampling rates of 5 – 20 samples/min and the result is an average value of neurotransmitter concentration. On the other hand, fast-scan cyclic voltammetry allows for monitoring of neurotransmitters every 10 milliseconds. But due to the nature of fast-scan cyclic voltammetry, there is a possibility that other compounds besides the ones desired get involved in the oxidation process thus skewing the results. Therefore, voltammetry is more useful for monitoring rapid changes occurring within small time windows (such as neurotransmitter release) while microdialysis is more suitable for measuring base levels of neurotransmitters over relatively long periods of time.

2.2.2. Existing Devices

There are several devices available for fast-scan voltammetry, such as Chem-Clamp[®] (Dagan Corporation, Minneapolis, MN), the WaveNano USB Potentiostat[®] (Pine Research Instrumentation, Durham, NC), and the EZstat-Pro[®] (NuVant Systems, Crown Point, IN). These devices are able to generate the voltage waveform to produce the desired oxidation at the electrode, and have the ability to monitor and record the current produced by the oxidation of the neurotransmitters at high enough speeds to dynamically capture changes in their chemical concentration dynamically. National Instruments produce high quality and expensive (~\$2000 per card) data acquisition cards for specifically this purpose, complete with software and user-friendly interfaces to set up the desired waveform and acquire the desired data (Figure 6). In addition, users must to purchase the LABVIEW[®] (National Instruments, Austin, TX) software required to collect and process the data from the cards making the total cost of the system >\$8000 for just the data acquisition. The computer and test setup required to perform the analysis becomes an additional expense adding to the financial burden of the FSCV system.

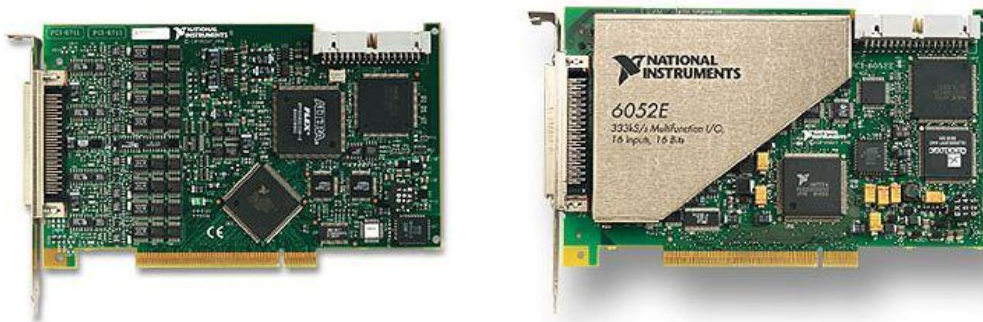


Figure 6: NI PCI-6711 High-Speed Analog Output card (left) and NI PCI-6052E High-Speed Analog Input card (right).

With a price point over \$8000 for the basic required equipment, the financial burden becomes the limiting step for many institutions wishing to utilize FSCV in their research or classrooms. Taking inspiration from the University of California, Santa Barbara with their open source Cheapstat design (Figure 7), we see that there is an opportunity to provide a open source alternative with FSCV technology for about \$200 (price of board manufacturing and components). Therefore, an increase in the availability of cheaper FSCV hardware would allow neuroscience analysis techniques to be demonstrated in the classroom along with allowing the opportunity for financially restricted institutions the opportunity to work with techniques that were previously cost-prohibitive.

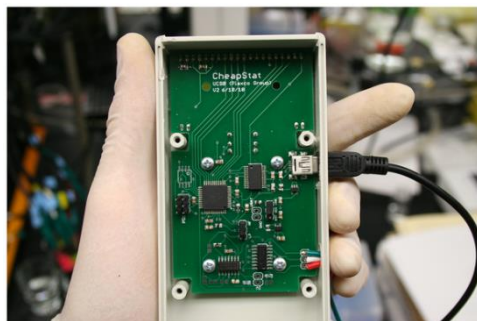


Figure 7: Cheapstat potentiostat developed by (University of California, Santa Barbara, 2011)

3. Specific Aims

The Specific Aims of this project are to develop a portable and cost-effective FSCV system for use in laboratory and classroom settings. Though cost effective, the system must be able to perform the most important tasks for FSCV accurately. These tasks include:

- The generation of the stimulus waveform
- Be able to monitor current flow in the electrode
- Amplification of the recorded current waveform
- The ability to convert the current waveform to digital form, and
- Have the recorded data available over USB to a computer for data analysis.

The first goal of the project was to create a microcontroller controlled prototype of the system that is able to generate the required stimulus ramp waveform through a Digital to Analog (DAC) converter and then read back the same stimulus ramp waveform through an Analog to Digital (ADC) converter. That would be a test to make sure that the ADC is able to correctly read a known voltage waveform. To perform this test, the basic firmware of the system would be developed and help expose any possible hardware issues such as communication failures between the microcontroller and the ADC.

After the prototype was exhaustively checked for hardware and software bugs, the device was iteratively tested using a dummy cell consisting of a resistor and capacitor in series by placing the dummy cell across the electrode leads. The dummy cell simulates the current generated by neurotransmitters. Using it to test the device would allow us to see if the small current could be measured accurately. After the dummy cell test, the device was tested in a laboratory setup in a mixture of dopamine in artificial cerebral spinal fluid.

Simultaneously, during the hardware development, software code was written in MATLAB[®] (Mathworks, Natick, MA) to acquire and interpret the data from the FSCV board. This is necessary not only as an end-product for data display and user interface, but also for troubleshooting and analysis during hardware development.

4. Methodology

In order to design the device so that it has all the functionality needed, the device will need to be broken down into its necessary components. This mapping of functionality will reinforce the design choices made and allow possible conflicts or problems to be brought to light. The simplification will clear up any unknown factors and outline the necessary design approach to create a working prototype and software system.

4.1. Hardware Design

Figure 8 (below) shows the functional block diagram of our FSCV system. In order to create a single system that can generate a voltage waveform to stimulate the electrode and then read in and interpret the resultant current waveform, an Analog to Digital Converter (ADC) and Digital to Analog Converter (DAC) were used. The DAC was an external integrated circuit (AD5662) while the ADC was a component of the microcontroller (ATxmega128A3). Electrical characteristics from the component datasheets have been included in Appendix I – Component Data Sheets. These were used in conjunction with several operation amplifiers (OPA2604) in order to create the appropriate waveform and interpret the resulting signal (Figure 8).

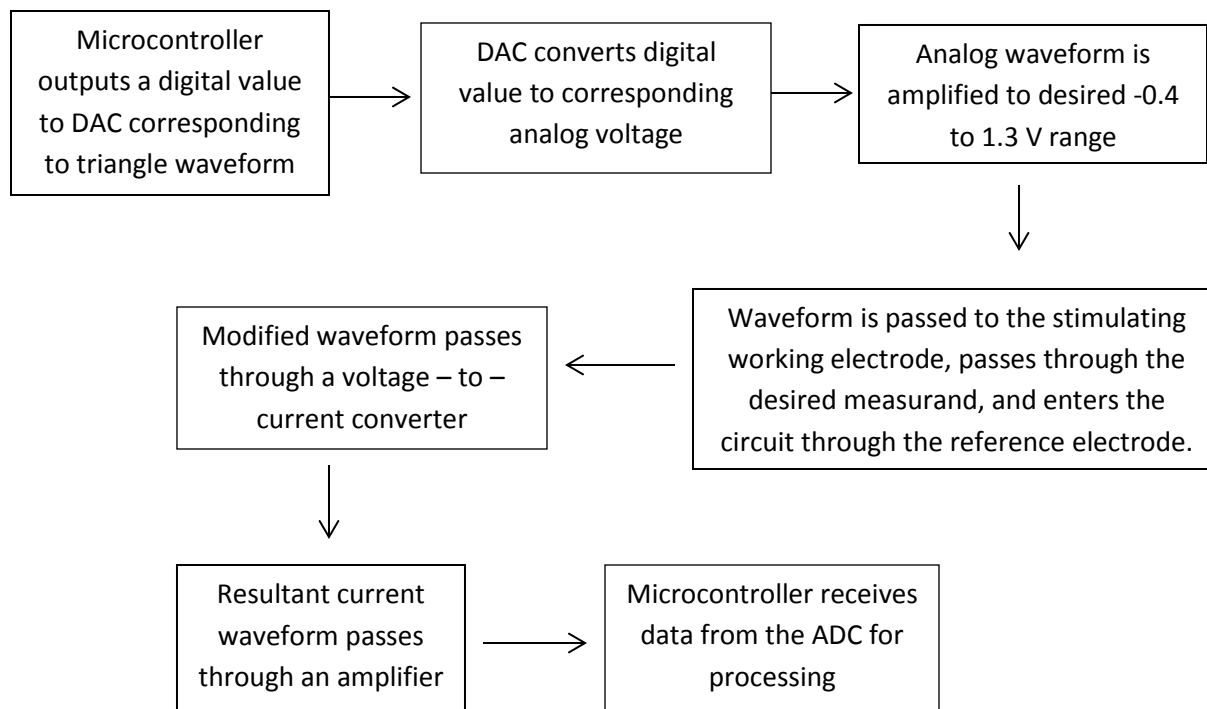


Figure 8: Functional Block diagram for hardware design

The microcontroller was programmed to produce the desired triangle wave to achieve the 400 V/sec rate of change from the resting potential to peak of the wave. As the DAC can only operate in a positive voltage range, an OPA2604 operational amplifier (op amp) was used to move the desired triangular waveform to the nominal voltage -0.4 V to 1.3 V using the configuration in Figure 9. The OPA2604 was chosen for its high input impedance, low leakage current, and its low noise characteristics. The specific DAC values for resting potential and peak value were calibrated to reach the specific desired values; the DAC values for the voltages after amplification were found to be 30000 for an output of -0.4 V, and 42000 for an output of 1.3V.

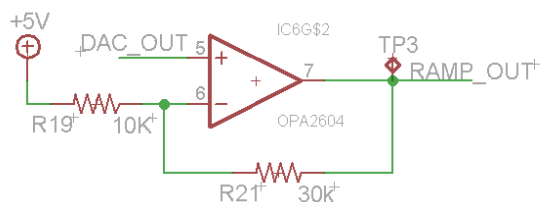


Figure 9: DAC Amplifier Design

After the waveform leaves the DAC amplifier, it is sent to the working electrode which is in direct contact with the measurand (dummy cell or test solution). The reference electrode is also suspended in the measurand and is able to record current changes due to the oxidation and reduction of the neurotransmitter being tested. In order for the ADC to accurately measure the current flowing through the working electrode, a current-to-voltage converter utilizing another op amp was built. The waveform representing electrode current was then sent to an amplifier with a gain of about seventeen. The measured currents are expected to be quite small (nanoamp range) and need substantial amplification in order to be seen properly. The ADC section of the amplifier circuit can be seen in Figure 10.

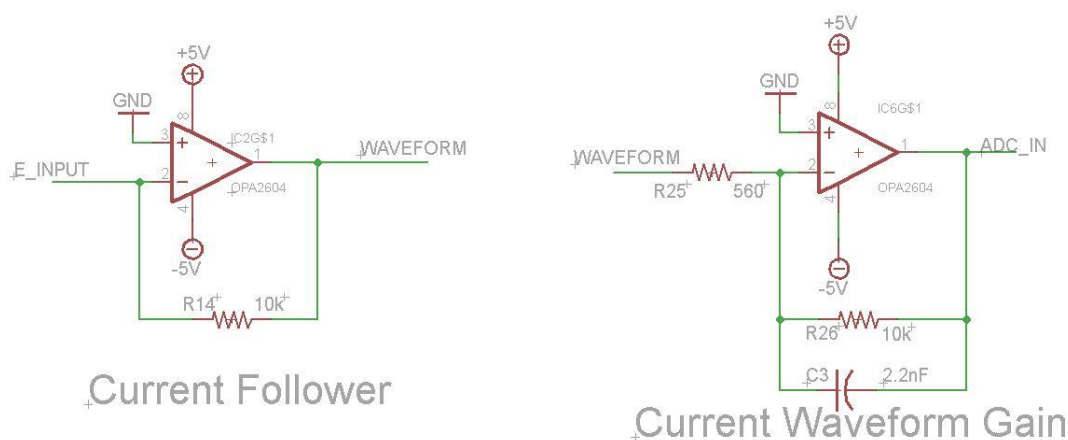


Figure 10: Current to Voltage Conversion and Amplification

4.2. Software Design

Figure 11 represents the software functional block diagram. All code has been provided in Appendix III – Matlab Code, Appendix IV – DAC Microcontroller Code, and Appendix V – ADC Microcontroller Code. The scope of software design included writing code that governed the operation of the board – such as generating the stimulus waveform and recording the values read from the ADC –along with programming that would run in conjunction with the board on the computer to receive the data from the board (Figure 11).

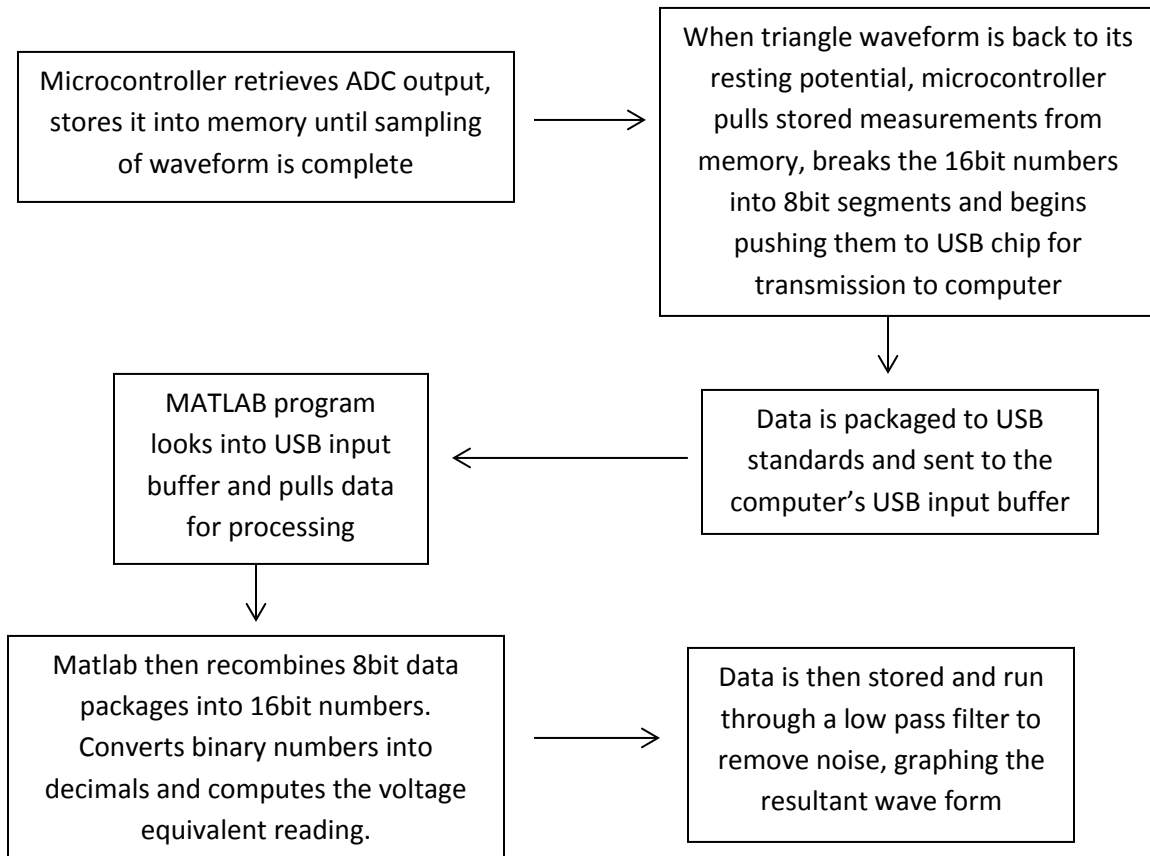


Figure 11: Functional block diagram for software

The first aspect of the software implemented was the programming of the microcontrollers. This controlled the performance of the DAC and ADC, along with triggering data collection and sending the data over USB to the computer. The microcontroller in charge of generating the waveform simply streams a set array of values to the DAC continuously. The array controlling the waveform was calibrated using an oscilloscope to make sure the triangle wave met the requirements a resting value of -0.4 and a peak of 1.3 V occurring at a 10 Hz rate with a duration of 8.5 ms.

With the data readily available over the USB port for the computer, the MATLAB program had to be able to collect the data as it was sent over the USB and translate the 8-bit transmission packages back into the 16-bit ADC measured values. The program recombined those bytes in the proper order in addition to verifying the data fell within an acceptable range. If the value resulted in an unexpected data value (outside the range of 5 V for example) a byte was thrown away as it was assumed there was a corruption or loss during transmission. The program then calculated the voltage equivalent for the values using equation (1) below as given by the xmega128 datasheet.

$$ADC\ Result = \frac{V_{inp} - V_{inn}}{V_{ref}} * 2047 \quad (1)$$

V_{ref} was set to be $3.3V / 1.6 = 2.06V$, and V_{inn} was connected to ground. The value for the reference voltage was chosen over the 1V reference due to testing, as the microcontroller had issues producing results at the speed required. The above equation gave the voltage that the ADC sampled, so to find the current at the electrode the current was calculated using the current follower equation (2), where V_o is the voltage output by the current-to-voltage

$$V_o = -iR_c \quad (2)$$

converter and R_c is the feedback resistor (10 k Ω). The waveform then passes through an amplifier which is governed by equation (3) that takes the output voltage from the current-to-

$$V_{inp} = -V_o \left(\frac{R_f}{R_i} \right) \quad (3)$$

voltage converter and boosts it with a gain governed by R_f and R_i which are 10 k Ω and 560 Ω respectively. This results in the voltage read at the ADC: V_{inp} . MATLAB uses the equation outlined in equation (4) to calculate the current at the electrode and then prints these values in graph form for verification.

$$i = -\frac{-V_{inp} \left(\frac{560\Omega}{10,000\Omega} \right)}{10,000\Omega} = V_{inp} * (5.6 * 10^{-6} \frac{1}{\Omega}) \quad (4)$$

5. Results

The first step of the project completed was the generation and output of the stimulating waveform. The code for the microcontroller generation was written and calibrated using an oscilloscope so that at the desired triangle wave occurred ten times a second and rested at -0.4 V and reached a peak of 1.3 V (Figure 12).

With the stimulating waveform completed, the next task was to verify that the ADC was able to read and report accurate values. The first test of the system involved just routing the pure triangle wave output to the ADC for testing. This involved not only getting the ADC apparatus up and running on the microcontroller but also the code for MATLAB to be written and be able to accept data from the board.

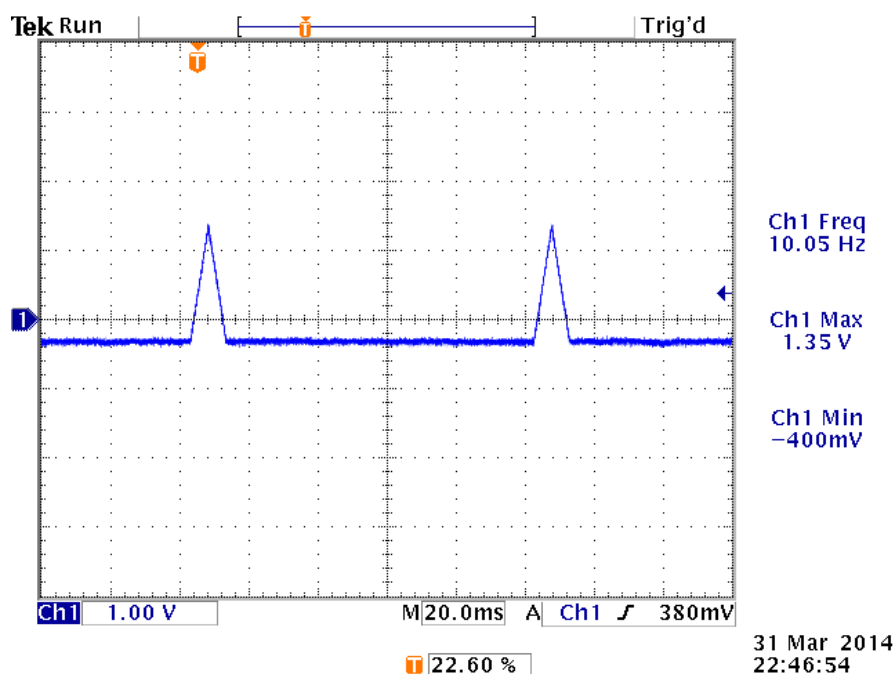


Figure 12: Device output - voltammetry stimulation waveform

The results from the MATLAB code are seen above in Figure 13 showing that the ADC is operational and collecting data. A simple low-pass filter with a corner frequency of 20 Hz was used to remove the high frequency content of the signal for a noise free triangle wave. The results show that the generated triangle waveform ranges from -0.373 to 1.34 V which correlates with the oscilloscope measurements of a resting potential of -0.4 V and a peak voltage of 1.3 V. However, because the currents being measured are very small, a discrepancy of millivolts is a problem – especially so on the negative voltage reading which differs from the oscilloscope readings by 30 millivolts. The device is able to capture the characteristic voltammetry waveform, which satisfied our needs.

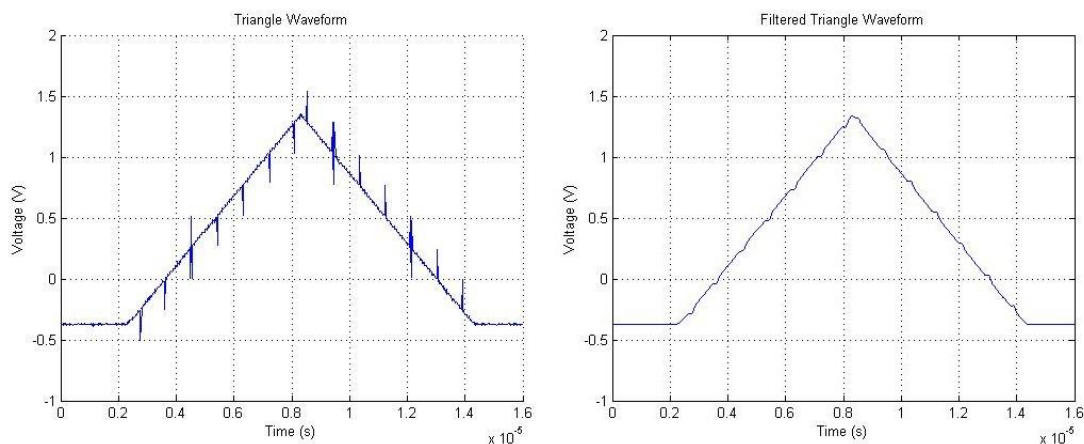


Figure 13: Raw data from ADC (left) and filtered data (right)

Next, this triangle waveform was used to stimulate the working electrode in the experimental setup involving a dummy cell consisting of a 100 k Ω resistor in series with a 1 nF capacitor.

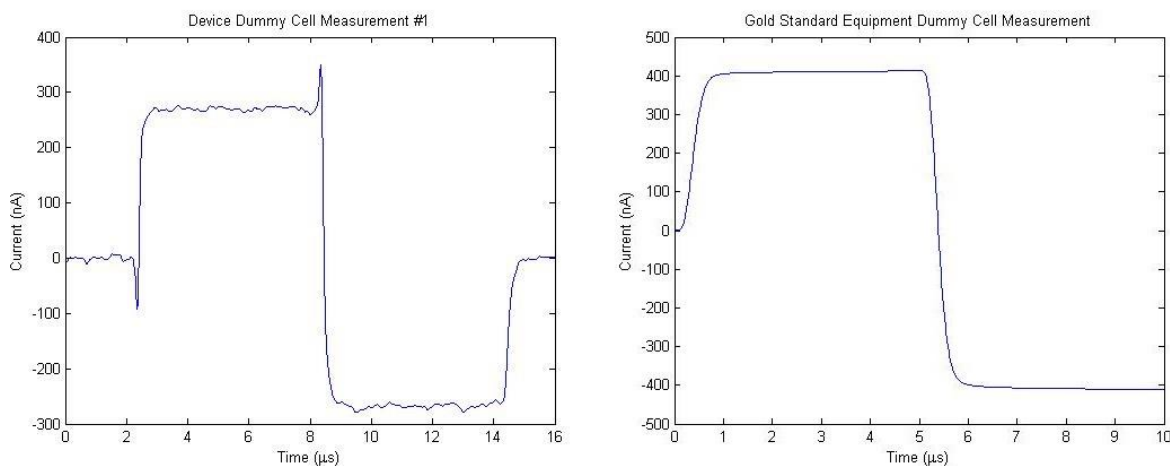


Figure 14: Result from device with dummy cell (left) compared to Gold Standard system dummy cell (right)

The dummy cell was measured on the Gold Standard lab equipment (Figure 14 – right) and the resulting waveform compared to that obtained from our device which is shown on the left

(Figure 14 – left). Note that while the results for the current measurements have about a hundred nanoamps of difference between them, the visual similarity is what was expected from testing the dummy cell. The current should flow in a positive direction during the ramp up from -0.4 to 1.3 V, then reverse as the voltage ramps back down again.

With the promising results from the dummy cell, the next step was to take the device into a lab setting where the device could be tested in a solution of artificial cerebral spinal fluid with a standard carbon fiber electrode (Figure 15). These device measurements can be compared to the gold standard recording seen in Figure 16 which shows the ideal measurement standard.

The different recordings show the different aspects of the device under test. Measurement #1 has noise in the recording that was reduced but not eliminated completely by the filter. Measurement #2 shows a tremendous peak current that – while it is expected, especially during the start of the recordings – goes much higher than the usual peak as seen in the other measurements. Measurements #3 and #4 demonstrate that the system is capable of getting very smooth and clear waveforms that show the characteristic voltage curve desired.

After the device was able to gather gathering the background current measurements reliably, different concentrations of dopamine were added to the artificial cerebral spinal fluid to see how well the device could detect the changes. The results can be seen in Figure 17 for dopamine concentrations of 1micromolar, 5micromolar, and 10micromolar with the background current outlined in red and the dopamine recordings superimposed over them in the blue.

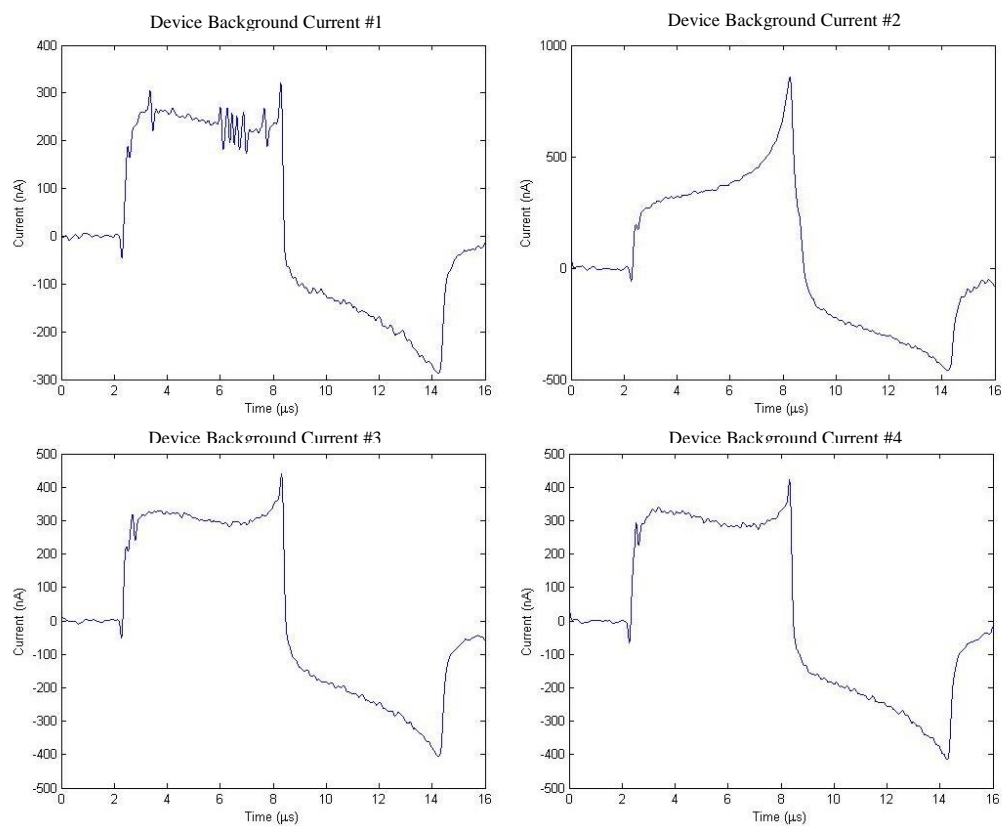


Figure 15: Background Current of the Electrode Measurements with Device

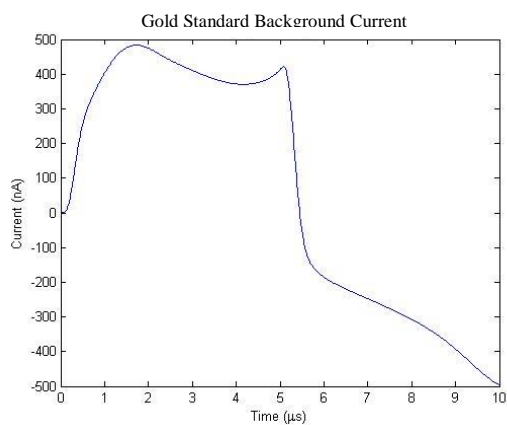


Figure 16: Gold Standard Equipment Background Current Measurement

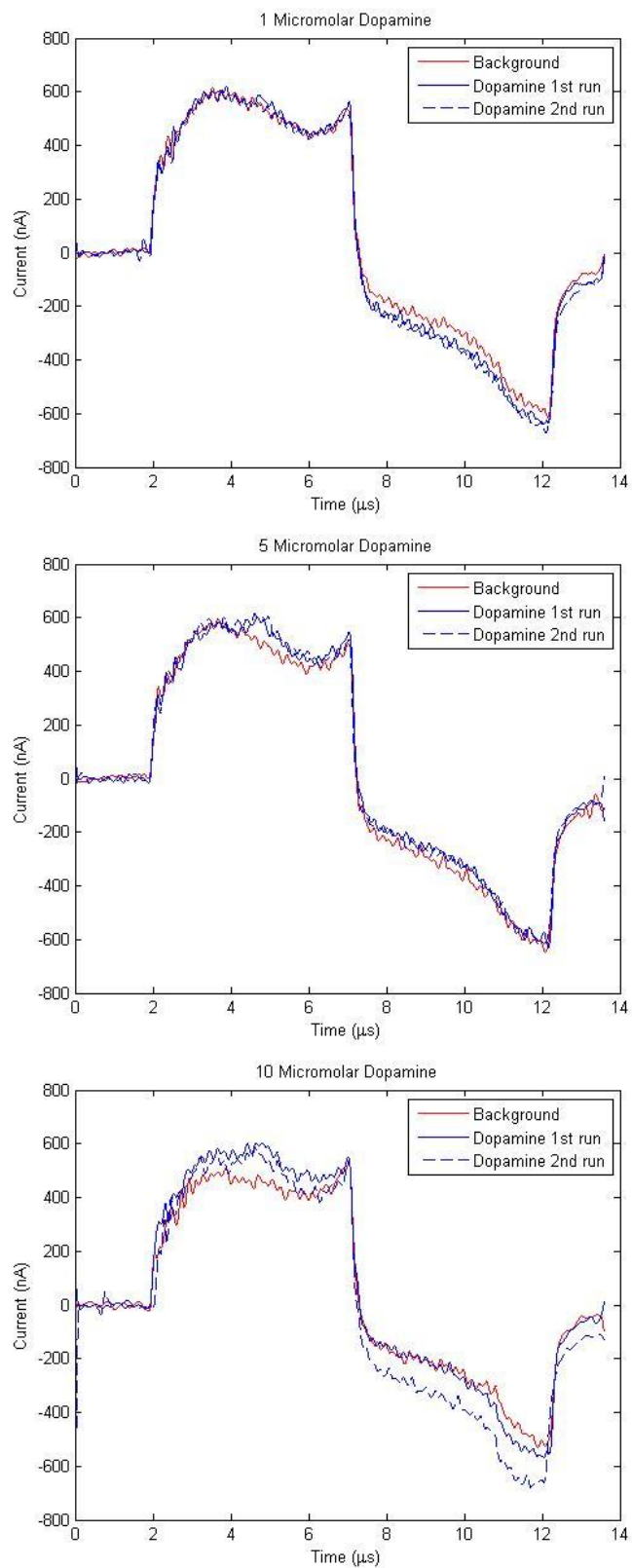


Figure 17: Dopamine Measurements taken with the device

To concisely relay the current differences in the dopamine measurements, the maximum differences have been compiled in Table 1. These measurements were taken at 4.5 microseconds and 10 microseconds for each recording, as this would correlate to the oxidation and reduction potentials of dopamine in the stimulus waveform.

Table 1: Dopamine Current Peak Measurements

	Positive Current Peak (nA)	Negative Current Peak (nA)
1 microM	25	70
5 microM	80	50
10 microM	120	120

6. Discussion

The hardware design got off to a misguided start. Taking over a previously started design attempt, there were several design and component choices that were taken for granted as correct – as there was no documentation from the previous designers. Therefore, while this iteration was intended to be a nearly finished product it in fact became a second prototype as several design flaws became apparent. These flaws remained undiscovered for so long due to the lack of an accurate output from the ADC, and the hardware design in the first prototype prevented the ADC from working properly.

The triangle wave output was able to be generated on the first prototype board, as it only ran through an amplifier to reach the electrode output. Writing the code for the microcontroller to output a set array to the DAC only involved measurement to find the correct values that would create a triangle wave of the correct specifications. However, working beyond that required the second prototype to be assembled.

With the second prototype designed and assembled with the design fixes that had been identified, the immediate need called for the ADC to be up and running. Unfortunately this was not as simple as the DAC, not only because the ADC process setup is very intricate but also due to the discovery that this family of microcontrollers has rather poorly supported documentation and code. In addition to getting the ADC working, MATLAB code had to be developed to see the values that the ADC was reading. The MATLAB code itself is rather simple, as gathering data from a USB port is similar to reading in a data file. To send the data involved sending the stored ADC values using a UART protocol from the microcontroller to the USB/UART integrated chip which formatted the data properly for transmission using USB protocols. This way, data gathered on the device could finally be seen by the user.

The ADC was tested using known waveforms and voltage values, such as the triangle waveform in Figure 13 to make sure the equation to convert the ADC measurements back into voltage readings was correct. As it can be seen in the figure, the waveform ranges from -0.373 to 1.34 V which correlates quite closely to the oscilloscope measured values. The discrepancy of 30mV on the negative reading suggests that the ADC conversion values may have an offset error for negative values. This is corroborated by the fact that when the ADC input is grounded, it reads a value of about -20mV. Through testing the ADC doesn't seem to have problems with purely positive readings but it does have an offset for negative readings. This was accommodated for, but further work would include mapping out the full ADC transfer function for analog voltages.

The next step was to get the board generating the stimulating waveform and recording the resulting measurements at the same time, as previously they had been running one at a time for

the purposes of debugging and development. During implementation it was found that the two functions took too many resources to have them functioning at the same time. Due to the time critical nature of the measurements and voltage waveform generation, it was found that they could not be operating at the same time without interfering with each other. In order to keep the triangle waveform within the proper parameters of 10 ms duration at 10 Hz, the microcontroller would have to deprioritize ADC sampling and storage or vice versa. This would cause the sampling rate to fall to unacceptable levels or the stimulating waveform to expand to such a degree as to nullify the experiment. Therefore, two microcontrollers were used so that each microcontroller would have a designated functionality: one to generate the stimulating waveform and one to record it. As the microcontroller is the most expensive singular component on the board, this will increase the cost of the device by ten dollars.

With the ADC and microcontrollers performing as desired, the waveform was used on a test dummy cell of a 100k Ω resistor and 1nF capacitor in series. When the measured voltages did not meet expectations, an in depth hardware review was performed. Reviewing the electrode interface, it was discovered that the design was based upon an amplifier headstage as opposed to a potentiostat (a potentiostat simply being the hardware to perform electrochemical experiments). A re-evaluation of the design necessary and the board was salvaged by simply using the existing op amps in different configurations to create a current-to-voltage converter and signal amplifier. This configuration was able to record the data shown in Figure 14 and Figure 15.

The results from the dummy cell show promise, as these closely match the signal from the gold standard equipment. The results from the laboratory testing with artificial cerebral spinal fluid show that our device is capable at capturing the characteristic voltammetric waveform.

While the measurement shows the voltammetric waveform quite clearly, the actual measurement is off by about a hundred nanoamps.

In testing the device in the lab, it was discovered that there was a thermal component that was causing the device to give inaccurate results. When the microcontrollers were active for a few minutes, the heat they generated caused their adc measurements to skew to give readings of 1000 nA. It was verified that the adc was receiving the proper waveform through an oscilloscope, and found that when left unplugged for a few seconds and then powered again to take a reading, the results were what was expected. This was a new development in the lab environment, as the boards had been left up and running for quite some time in other environments with no problem. Therefore, cooling methods will have to be implemented in the future.

When it came to the actual dopamine measurements, the device was able to show a very definite positive oxidation current for the 5 micromolar and 10 micromolar concentrations, with a possible slight reading on the 1 micromolar. However when it came to recording the negative reduction currents, the results were more indistinct as there was not a definite “bump” on the waveform that correlated to the dopamine oxidation. Ideally, as the concentration gradient increased the current readings would increase linearly as well so that the 5 micromolar reading would be five times what the 1 micromolar reading was. Looking at the positive oxidation current measurements in Table 1, they are not far off from a linear relationship. The negative current measurements however are not as reliable, and this may be due to the fact that the reduction current is usually smaller than the oxidation measurement.

Our device was developed to give a more economical solution to the gold standard for FSCV. The device successfully does this and has enough resolution to still be able to see the important voltammetry effects. The device results are not perfect, as there are some artifacts from ringing in the results and the current measurement is inconsistent with the gold standard. However, it does provide the characteristic current waveform that is important for voltammetry and is able to show a visible difference in recordings in the presence of dopamine.

7. Future Work

There are several different aspects of this project that can be improved upon, both from a hardware and software prospective. This project did result in a final board design by resolving several errors that were exposed in the design used, but a complete integrated board still needs to be built and tested. Instead of having two independent microcontrollers, it would be ideal to have an independent ADC that would automatically shift the data values directly to a memory chip. Currently the memory available on the xmega128 microcontroller can only handle enough for one triangle wave recording, while to be fully useful it must be able to store measurements for at least 10 triangle waves. In order to gather a data set, the reset button must be pressed. Ideally the data would require no user interaction and gather all the data sets automatically as soon as the user pressed one button to start collecting data.

For the software, instead of relying on a MATLAB application it would be ideal to have an open source application, such as SciLab[®] (Scilab Enterprises, Versailles, France) to collect the data rather than needing a MATLAB license. The software also still needs to be able to handle 10 recordings of the waveform and output them all together in order to show levels of dopamine

over time. In addition, a desirable feature of the independent application would be to allow the user to change the stimulus waveform used, duration, frequency, etc. Then they would press a button in the application and the hardware would follow the data sent from the PC application. As it is, the microcontroller is running a single constant triangular waveform and constantly reading the data when powered.

In addition, a case to hold the device and keep it cooled will be required to make it able to withstand transportation without worry. The case will also need to factor in methods to keep the microcontrollers cooled, as that would affect their reading greatly if allowed to heat up.

8. Conclusion

The device has achieved the initial Specific Aims. It has been able to successfully generate the electrolysis waveform and monitor the current moving through the electrode, amplify it, and convert it to digital information for analysis. The recorded data points are available through MATLAB, allowing for data analysis and display using the programs functions. The ability of the device to record the exact current flow through the electrodes is lacking, but it gives the desired results with enough resolution to be useful. It is able to show the user the general form of the data, if not exact values with good precision. However, as it is an order of magnitude lower in price than the gold standard equipment, the precision loss is acceptable to demonstrate the characteristic voltage waveform of voltammetry and the device can be utilized to test electrodes. The device shows the feasibility of the design to capture voltammetric current waveforms cheaply, and can be further refined to give precise current measurements.

Bibliography

- Chang, W. C., Keller, C. G., & Sretavan, D. W. (2006, April 15). Isolation of neuronal substructures and precise neural microdissection using a nanocutting device. *Isolation of neuronal substructures and precise neural microdissection using a nanocutting device*, 152(1-2), 83-90. Retrieved March 8, 2014
- Chara, P. J. (2010). Neurotransmitters. (N. A. Piotrowski, Ed.) *Salem Health: Psychology & Mental Health*, 3, 1291-1293. Retrieved March 8, 2014
- Davis, K. L., Kahn, R. S., & al, e. (1991). Dopamine in schizophrenia: A review and reconceptualization. *The American Journal of Psychiatry*, 148(11), 1474-86.
- del Campo, N., Chamberlain, S. R., Sahakian, B. J., & Robbins, T. W. (2011, June 15). The Roles of Dopamine and Noadrenaline in the Pathophysiology and Treatment of Attention-Deficit/Hyperactivity Disorder. *Biological Psychiatry*, 69(12), 145-157. doi:<http://dx.doi.org/10.1016/j.biopsych.2011.02.036>
- Garrus, P. A., Kilpatrick, M., Bunin, M. A., Michael, D., & al, e. (1999). Dissociation of dopamine release in the nucleus accumbens from intracranial self-stimulation. *Nature*, 398(6722), 67-9. Retrieved March 8, 2014
- Helgeson, J. S. (2010). Inhibitory and Excitatory Impulses. (N. A. Piotrowski, Ed.) *Salem Health: Psychology & Mental Health*, 3, 1007-1011. Retrieved March 8, 2014
- Hisahara, S., & Shimohama, S. (2011). Dopamine Receptors and Parkinson's Disease. *International Journal of Medicinal Chemistry*, vol. 2011, 16 pages. doi:10.1155/2011/403039
- Jaquins-Gerstl, A., & Michael, A. C. (2009, October 15). Comparison of the brain penetration injury associated with microdialysis and voltammetry. *Journal of Neuroscience Methods*, 183(2), 127-135. Retrieved March 8, 2014
- Jones, S. R., Gainetdinov, R. R., & Marc, C. G. (1999). Application of microdialysis and voltammetry to assess dopamine functions in genetically altered mice: correlation with locomotor activity. *Psychopharmacology*(147), 30-32.
- Korpi, E. R., Kleinman, J. E., Goodman, S. I., & Wyatt, R. J. (1987, December). Neurotransmitter amino acids in post-mortem brains of chronic schizophrenic patients. *Psychiatry Research*, 22(4), 291-301. Retrieved March 8, 2014
- Kottegoda, S., Shaik, I., & Shippy, S. A. (2002, November 15). Demonstration of low flow push-pull perfusion. *Journal of Neuroscience Methods*, 121(1), 93-101.
- Mitchell, J. F. (1963). The Spontaneous and Evoked Release of Acetylcholine from the Cerebral Cortex. *The Journal of physiology*, 165, 98-116.

- Moroni, F., & Pepeu, G. (1984). The cortical cup technique. *Measurement of neurotransmitter release in vivo*, 63-105.
- Muller, M. (2002). Microdialysis. *British Medical Journal*, 324(7337), 588-591.
- National Institutes of Health. (n.d.). *Neurons, Brain Chemistry, and Neurotransmission*. Retrieved March 8, 2014, from The Brain: Understanding Neurobiology: <http://science.education.nih.gov/supplements/nih2/addiction/guide/lesson2-1.htm>
- Syslová, K., Rambousek, L., Bubeníková - Valešová, V., Šlamberová, R., Novotný, P., & Kačer, P. (2012). *Dopamine Analysis in Neuroscience Research*. (E. Fujii, & Y. Kudo, Eds.) Hauppague, NY: Nova Science Publishers.
- Tayebati, S. K., Lokhandwala, M. F., & Amenta, F. (2011, August). Dopamine and Vascular Dynamics Control: Present Status and Future Perspectives. *CURRENT NEUROVASCULAR RESEARCH*, 246-257.
- UCLA Department of Psychology. (n.d.). *In Vivo Fast-Scan Cyclic Voltammetry*. (UCLA) Retrieved from Wassum Lab: <http://wassumlab.psych.ucla.edu/research/in-vivo-fast-scan-cyclic-voltammetry/>
- University of California, Santa Barbara. (2011). *Building a Cheapstat*. Retrieved March 10, 2014, from UCSB Chemistry and Biochemistry: <http://web.chem.ucsb.edu/~kwp/cheapstat/>
- Waxman, S. G. (08/2009). *Clinical Neuroanatomy (26th Edition)*. New York, NY: McGraw-Hill Professional Publishing.

Appendix I – Component Data Sheets

Features

- High-performance, Low-power 8/16-bit Atmel® AVR® XMEGA™ Microcontroller
- Non-volatile Program and Data Memories
 - 64 KB - 256 KB of In-System Self-Programmable Flash
 - 4 KB - 8 KB Boot Code Section with Independent Lock Bits
 - 2 KB - 4 KB EEPROM
 - 4 KB - 16 KB Internal SRAM
- Peripheral Features
 - Four-channel DMA Controller with support for external requests
 - Eight-channel Event System
 - Seven 16-bit Timer/Counters
 - Four Timer/Counters with 4 Output Compare or Input Capture channels
 - Three Timer/Counters with 2 Output Compare or Input Capture channels
 - High Resolution Extensions on all Timer/Counters
 - Advanced Waveform Extension on one Timer/Counter
 - Seven USARTs
 - IrDA Extension on 1 USART
 - AES and DES Crypto Engine
 - Two Two-wire Interfaces with dual address match (I²C and SMBus compatible)
 - Three SPI (Serial Peripheral Interfaces)
 - 16-bit Real Time Counter with Separate Oscillator
 - Two Eight-channel, 12-bit, 2 Msps Analog to Digital Converters
 - One Two-channel, 12-bit, 1 Msps Digital to Analog Converter
 - Four Analog Comparators with Window compare function
 - External Interrupts on all General Purpose I/O pins
 - Programmable Watchdog Timer with Separate On-chip Ultra Low Power Oscillator
- Special Microcontroller Features
 - Power-on Reset and Programmable Brown-out Detection
 - Internal and External Clock Options with PLL
 - Programmable Multi-level Interrupt Controller
 - Sleep Modes: Idle, Power-down, Standby, Power-save, Extended Standby
 - Advanced Programming, Test and Debugging Interfaces
 - JTAG (IEEE 1149.1 Compliant) Interface for test, debug and programming
 - PDI (Program and Debug Interface) for programming, test and debugging
- I/O and Packages
 - 50 Programmable I/O Lines
 - 64-lead TQFP
 - 64-pad QFN
- Operating Voltage
 - 1.6 – 3.6V
- Speed performance
 - 0 – 12 MHz @ 1.6 – 3.6V
 - 0 – 32 MHz @ 2.7 – 3.6V

Typical Applications

- | | | |
|----------------------|-------------------|----------------------------------|
| • Industrial control | • Climate control | • Hand-held battery applications |
| • Factory automation | • ZigBee | • Power tools |
| • Building control | • Motor control | • HVAC |
| • Board control | • Networking | • Metering |
| • White Goods | • Optical | • Medical Applications |



8/16-bit AVR® XMEGA A3 Microcontroller

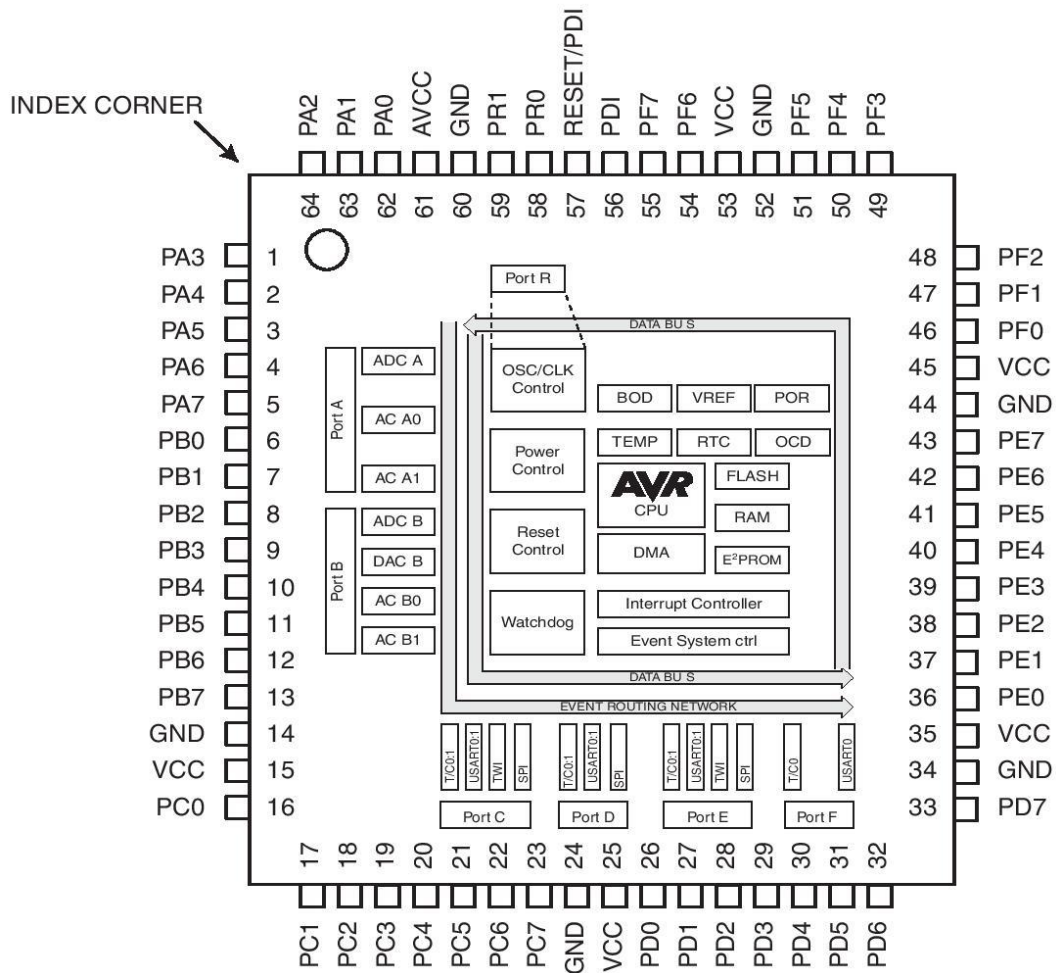
ATxmega256A3
ATxmega192A3
ATxmega128A3
ATxmega64A3

8068T-AVR-12/10



2. Pinout/Block Diagram

Figure 2-1. Block diagram and pinout.



- Notes:
1. For full details on pinout and alternate pin functions refer to "Pinout and Pin Functions" on page 49.
 2. The large center pad underneath the QFN/MLF package should be soldered to ground on the board to ensure good mechanical stability.

3. Overview

The Atmel® AVR® XMEGA™ A3 is a family of low power, high performance and peripheral rich CMOS 8/16-bit microcontrollers based on the AVR enhanced RISC architecture. By executing powerful instructions in a single clock cycle, the XMEGA A3 achieves throughputs approaching 1 Million Instructions Per Second (MIPS) per MHz allowing the system designer to optimize power consumption versus processing speed.

The AVR CPU combines a rich instruction set with 32 general purpose working registers. All the 32 registers are directly connected to the Arithmetic Logic Unit (ALU), allowing two independent registers to be accessed in one single instruction, executed in one clock cycle. The resulting architecture is more code efficient while achieving throughputs many times faster than conventional single-accumulator or CISC based microcontrollers.

The XMEGA A3 devices provide the following features: In-System Programmable Flash with Read-While-Write capabilities, Internal EEPROM and SRAM, four-channel DMA Controller, eight-channel Event System, Programmable Multi-level Interrupt Controller, 50 general purpose I/O lines, 16-bit Real Time Counter (RTC), seven flexible 16-bit Timer/Counters with compare modes and PWM, seven USARTs, two Two Wire Serial Interfaces (TWIs), three Serial Peripheral Interfaces (SPIs), AES and DES crypto engine, two 8-channel 12-bit ADCs with optional differential input with programmable gain, one 2-channel 12-bit DACs, four analog comparators with window mode, programmable Watchdog Timer with separate Internal Oscillator, accurate internal oscillators with PLL and prescaler and programmable Brown-Out Detection.

The Program and Debug Interface (PDI), a fast 2-pin interface for programming and debugging, is available. The devices also have an IEEE std. 1149.1 compliant JTAG test interface, and this can also be used for On-chip Debug and programming.

The XMEGA A3 devices have five software selectable power saving modes. The Idle mode stops the CPU while allowing the SRAM, DMA Controller, Event System, Interrupt Controller and all peripherals to continue functioning. The Power-down mode saves the SRAM and register contents but stops the oscillators, disabling all other functions until the next TWI or pin-change interrupt, or Reset. In Power-save mode, the asynchronous Real Time Counter continues to run, allowing the application to maintain a timer base while the rest of the device is sleeping. In Standby mode, the Crystal/Resonator Oscillator is kept running while the rest of the device is sleeping. This allows very fast start-up from external crystal combined with low power consumption. In Extended Standby mode, both the main Oscillator and the Asynchronous Timer continue to run. To further reduce power consumption, the peripheral clock for each individual peripheral can optionally be stopped in Active mode and Idle sleep mode.

The device is manufactured using Atmel's high-density nonvolatile memory technology. The program Flash memory can be reprogrammed in-system through the PDI or JTAG. A Bootloader running in the device can use any interface to download the application program to the Flash memory. The Bootloader software in the Boot Flash section will continue to run while the Application Flash section is updated, providing true Read-While-Write operation. By combining an 8/16-bit RISC CPU with In-System Self-Programmable Flash, the Atmel XMEGA A3 is a powerful microcontroller family that provides a highly flexible and cost effective solution for many embedded applications.

The XMEGA A3 devices are supported with a full suite of program and system development tools including: C compilers, macro assemblers, program debugger/simulators, programmers, and evaluation kits.



2.7 V to 5.5 V, 250 μ A, Rail-to-Rail Output 16-Bit *nano*DAC™ in a SOT-23

AD5662

FEATURES

- Low power (250 μ A @ 5 V) single 16-bit *nano*DAC
- 12-bit accuracy guaranteed
- Tiny 8-lead SOT-23/MSOP package
- Power-down to 480 nA @ 5 V, 100 nA @ 3 V
- Power-on reset to zero scale/midscale
- 2.7 V to 5.5 V power supply
- Guaranteed 16-bit monotonic by design
- 3 power-down functions
- Serial interface with Schmitt-triggered inputs
- Rail-to-rail operation
- SYNC interrupt facility
- Temperature range -40°C to $+125^{\circ}\text{C}$
- Qualified for automotive applications

APPLICATIONS

- Process control
- Data acquisition systems
- Portable battery-powered instruments
- Digital gain and offset adjustment
- Programmable voltage and current sources
- Programmable attenuators

GENERAL DESCRIPTION

The AD5662, a member of the *nano*DAC family, is a low power, single, 16-bit buffered voltage-out DAC that operates from a single 2.7 V to 5.5 V supply and is guaranteed monotonic by design.

The AD5662 requires an external reference voltage to set the output range of the DAC. The part incorporates a power-on reset circuit that ensures the DAC output powers up to 0 V (AD5662x-1) or to midscale (AD5662x-2), and remains there until a valid write takes place. The part contains a power-down feature that reduces the current consumption of the device to 480 nA at 5 V and provides software-selectable output loads while in power-down mode.

The low power consumption of this part in normal operation makes it ideally suited to portable battery-operated equipment. The power consumption is 0.75 mW at 5 V, going down to 2.4 μ W in power-down mode.

The AD5662's on-chip precision output amplifier allows rail-to-rail output swing to be achieved. For remote sensing applications, the output amplifier's inverting input is available to the user.

Rev. A

Information furnished by Analog Devices is believed to be accurate and reliable. However, no responsibility is assumed by Analog Devices for its use, nor for any infringements of patents or other rights of third parties that may result from its use. Specifications subject to change without notice. No license is granted by implication or otherwise under any patent or patent rights of Analog Devices. Trademarks and registered trademarks are the property of their respective owners.

FUNCTIONAL BLOCK DIAGRAM

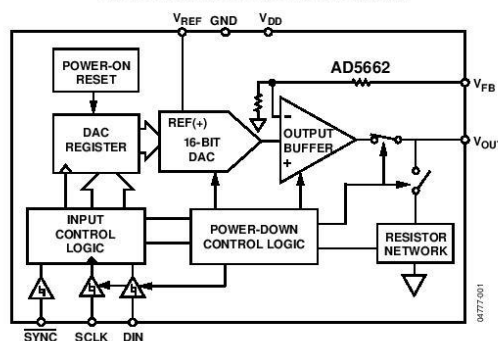


Figure 1.

The AD5662 uses a versatile 3-wire serial interface that operates at clock rates up to 30 MHz, and is compatible with standard SPI®, QSPI®, MICROWIRE™, and DSP interface standards.

PRODUCT HIGHLIGHTS

- 16-bit DAC—12-bit accuracy guaranteed.
- Available in 8-lead SOT-23 and 8-lead MSOP packages.
- Low power. Typically consumes 0.42 mW at 3 V and 0.75 mW at 5 V.
- Power-on reset to zero scale or to midscale.
- 10 μ s max settling time.

RELATED DEVICES

Part No.	Description
AD5620/AD5640/AD5660	3 V/5 V 12-/14-/16-bit DAC with internal reference in SOT-23

One Technology Way, P.O. Box 9106, Norwood, MA 02062-9106, U.S.A.
Tel: 781.329.4700 www.analog.com
Fax: 781.326.8703 ©2005–2010 Analog Devices, Inc. All rights reserved.

SPECIFICATIONS

$V_{DD} = 2.7\text{ V to }5.5\text{ V}$; $R_L = 2\text{ k}\Omega$ to GND; $C_L = 200\text{ pF}$ to GND; $V_{REF} = V_{DD}$; all specifications T_{MIN} to T_{MAX} , unless otherwise noted.

Table 1.

Parameter	A Grade			B Grade			Unit	Y Version ¹ Conditions/Comments	
	Min	Typ	Max	Min	Typ	Max			
STATIC PERFORMANCE ²									
Resolution	16			16			Bits	See Figure 4 Guaranteed monotonic by design See Figure 5 All 0s loaded to DAC register All 1s loaded to DAC register Of FSR/°C DAC code = midscale; V _{DD} = 5 V/3 V ±10%	
Relative Accuracy		±8	±32		±8	±16	LSB		
Differential Nonlinearity			±1			±1	LSB		
Zero Code Error		2	10		2	10	mV		
Full-Scale Error		−0.2	−1		−0.2	−1	% FSR		
Offset Error			±10			±10	mV		
Gain Error			±1.5			±1.5	% FSR		
Zero Code Error Drift ³		±2			±2		μV/°C		
Gain Temperature Coefficient ³		±2.5			±2.5		ppm		
DC Power Supply Rejection Ratio ³		−100			−100		dB		
OUTPUT CHARACTERISTICS ³									
Output Voltage Range	0		V _{DD}	0		V _{DD}	V	¼ to ¾ scale change settling to ±2 LSB R _L = 2 kΩ; 0 pF < C _L < 200 pF ¼ to ¾ scale R _L = ∞ R _L = 2 kΩ DAC code = midscale, 10 kHz DAC code = midscale V _{REF} = 2 V ± 300 mV p-p, f = 5 kHz 1 LSB change around major carry V _{DD} = 5 V, 3 V Coming out of power-down mode V _{DD} = 5 V, 3 V	
Output Voltage Settling Time		8	10		8	10	μs		
Slew Rate		1.5			1.5		V/μs		
Capacitive Load Stability		2			2		nF		
		10			10		nF		
Output Noise Spectral Density ⁴		100			100		nV/√Hz		
Output Noise (0.1 Hz to 10 Hz) ⁴		10			10		μV p-p		
Total Harmonic Distortion (THD) ⁴		−80			−80		dB		
Digital-to-Analog Glitch Impulse		5			5		nV-s		
Digital Feedthrough		0.1			0.1		nV-s		
DC Output Impedance		0.5			0.5		Ω		
Short-Circuit Current ⁴		30			30		mA		
Power-Up Time		4			4		μs		
REFERENCE INPUT ³									
Reference Current		40	75		40	75	μA		V _{REF} = V _{DD} = 5 V V _{REF} = V _{DD} = 3.6 V
		30	50		30	50	μA		
Reference Input Range ⁵	0.75		V _{DD}	0.75		V _{DD}	V		
Reference Input Impedance		125			125		kΩ		
LOGIC INPUTS ³									
Input Current			±2			±2	μA	All digital inputs V _{DD} = 5 V, 3 V V _{DD} = 5 V, 3 V	
V _{INL} , Input Low Voltage			0.8			0.8	V		
V _{INH} , Input High Voltage	2			2			V		
Pin Capacitance		3			3		pF		

AD5662

Parameter	A Grade			B Grade			Unit	Y Version ¹ Conditions/Comments
	Min	Typ	Max	Min	Typ	Max		
POWER REQUIREMENTS								
V _{DD}	2.7		5.5	2.7		5.5	V	All digital inputs at 0 V or V _{DD}
I _{DD} (Normal Mode)								DAC active and excluding load current
V _{DD} = 4.5 V to 5.5 V		150	250		150	250	μA	V _H = V _{DD} and V _{IL} = GND
V _{DD} = 2.7 V to 3.6 V		140	225		140	225	μA	V _H = V _{DD} and V _{IL} = GND
I _{DD} (All Power-Down Modes)								
V _{DD} = 4.5 V to 5.5 V		0.48	1		0.48	1	μA	V _H = V _{DD} and V _{IL} = GND
V _{DD} = 2.7 V to 3.6 V		0.1	0.375		0.1	0.375	μA	V _H = V _{DD} and V _{IL} = GND
POWER EFFICIENCY								
I _{OUT} /I _{DD}		90			90		%	I _{LOAD} = 2 mA, V _{DD} = 5 V

¹ Temperature range is as follows: Y version: -40°C to +125°C, typical at +25°C.

² DC specifications tested with the outputs unloaded, unless otherwise stated. Linearity calculated using a reduced code range of 512 to 65024.

³ Guaranteed by design and characterization; not production tested.

⁴ Output unloaded.

⁵ Reference input range at ambient where ±1 LSB max DNL specification is achievable.



1.5A CMOS LDO

The AME8815 family of linear regulators feature low quiescent current (45µA typ.) with low dropout voltage, making them ideal for battery applications. It is available in TO-252, SOT-223, TO-263 and TO-220 packages.

These rugged devices have both Thermal Shutdown, and Current Fold-back to prevent device failure under the "Worst" operating conditions.

- Very Low Dropout Voltage
- Guaranteed 1.5A Output
- Accurate to within 1.5%
- 45µA Quiescent Current Typically
- Over-Temperature Shutdown
- Current Limiting
- Short Circuit Current Fold-back
- Low Temperature Coefficient
- All AME' s Lead Free Products Meet RoHS Standards

- Instrumentation
- Portable Electronics
- Wireless Devices
- PC Peripherals
- Battery Powered Widgets



AME8815

1.5A CMOS LDO

■ Electrical Specifications

$V_{IN} = V_{O(NOM)} + 2V$, $T_A = 25^\circ C$ unless otherwise noted

Parameter	Symbol	Test Condition		Min	Typ	Max	Units
Input Voltage	V _{IN}			Note 1		7	V
Output Voltage Accuracy	V _O	I _O =1mA		-1.5		1.5	%
Dropout Voltage	V _{DROPOUT}	I _O =1.5A V _O =V _{O(NOM)} -2.0%	1.4V<V _{O(NOM)} <=2.0V		See chart	1300	mV
			2.0V<V _{O(NOM)} <=2.8V			800	
			2.8V<V _{O(NOM)}			600	
Output Current	I _O	V _O >1.2V		1500			mA
Current Limit	I _{LIM}	V _O >1.2V		1500	2000		mA
Short Circuit Current	I _{SC}	V _{IN} = V _{O(NOM)} +1V, V _O <0.4V			750		mA
Quiescent Current	I _Q	I _O =0mA			45	70	μA
Ground Pin Current	I _{GND}	I _O =1mA to 1500mA			45		μA
Line Regulation	REG _{LINE}	I _O =1mA V _{IN} =V _O +1 to V _O +2	V _O < 2.0V	-0.15		0.15	%
			4.0V > V _O >= 2.0V	-0.1	0.02	0.1	%
			4.0V <= V _O	-0.4		0.4	%
Load Regulation	REG _{LOAD}	I _O =1mA to 1500mA		-1	0.2	1	%
Over Temperature Shutdown	OTS				150		°C
Over Temperature Hysteresis	OTH				30		°C
V _O Temperature Coefficient	TC				30		ppm/°C
Power Supply Rejection	PSRR	I _O =100mA C _O =4.7μF	f=100Hz		70		dB
			f=1kHz		50		
			f=10kHz		20		
Output Voltage Noise	eN	f=10Hz to 100kHz I _O =10mA	Co=4.7μF		30		μVrms

Note1: $V_{IN(min)} = V_{OUT} + V_{DROPOUT}$



LD1117xx

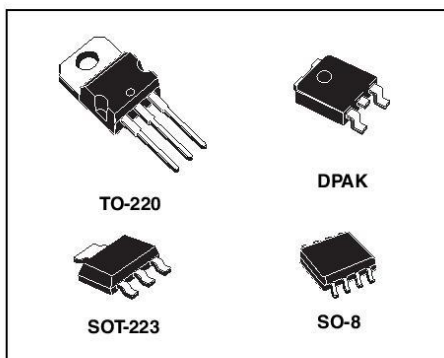
Adjustable and fixed low drop positive voltage regulator

Features

- Low dropout voltage (1 V typ.)
- 2.85 V device performances are suitable for SCSI-2 active termination
- Output current up to 800 mA
- Fixed output voltage of: 1.2 V, 1.8 V, 2.5 V, 3.0 V, 3.3 V, 5.0 V
- Adjustable version availability ($V_{REF} = 1.25$ V)
- Internal current and thermal limit
- Available in ± 1 % (at 25 °C) and 2 % in full temperature range
- Supply voltage rejection: 75 dB (typ.)

Description

The LD1117 is a low drop voltage regulator able to provide up to 800 mA of output current, available even in adjustable version ($V_{REF} = 1.25$ V). Concerning fixed versions, are offered the following output voltages: 1.2 V, 1.8 V, 2.5 V, 2.85 V, 3.0 V, 3.3 V and 5.0 V. The 2.85 V type is ideal for SCSI-2 lines active termination. The device is supplied in: SOT-223, DPAK, SO-8 and TO-220. The SOT-223 and DPAK surface mount packages optimize the thermal characteristics even offering a relevant space saving effect. High efficiency is assured by NPN pass transistor. In fact in this case, unlike than PNP one, the quiescent current flows mostly into the load. Only a very common 10 μ F minimum capacitor is needed for stability.



On chip trimming allows the regulator to reach a very tight output voltage tolerance, within ± 1 % at 25 °C. The adjustable LD1117 is pin to pin compatible with the other standard. Adjustable voltage regulators maintaining the better performances in terms of drop and tolerance.

Table 1. Device summary

Part numbers		
LD1117XX12	LD1117XX25C	LD1117XX50C
LD1117XX12C	LD1117XX30	LD1117XX
LD1117XX18	LD1117XX33	LD1117XXC
LD1117XX18C	LD1117XX33C	
LD1117XX25	LD1117XX50	

4 Schematic application

Figure 3. Application circuit (for 1.2 V)

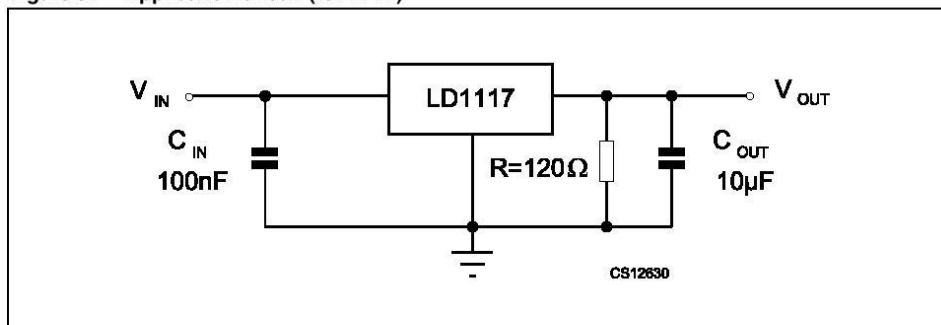
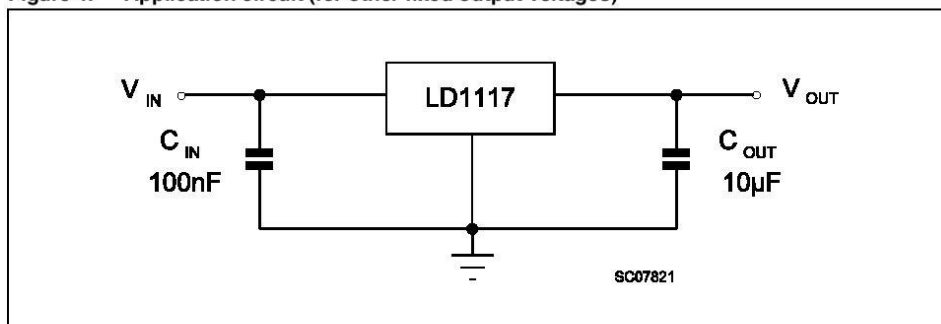


Figure 4. Application circuit (for other fixed output voltages)



Refer to the test circuits, $T_J = 0$ to $125\text{ }^{\circ}\text{C}$, $C_O = 10\text{ }\mu\text{F}$, unless otherwise specified.

Table 6. Electrical characteristics of LD1117#25

Symbol	Parameter	Test condition	Min.	Typ.	Max.	Unit
V_O	Output voltage	$V_{in} = 4.5\text{ V}$, $I_O = 10\text{ mA}$, $T_J = 25\text{ }^{\circ}\text{C}$	2.475	2.5	2.525	V
V_O	Output voltage	$I_O = 0$ to 800 mA , $V_{in} = 3.9$ to 10 V	2.45		2.55	V
ΔV_O	Line regulation	$V_{in} = 3.9$ to 10 V , $I_O = 0\text{ mA}$		1	6	mV
ΔV_O	Load regulation	$V_{in} = 3.9\text{ V}$, $I_O = 0$ to 800 mA		1	10	mV
ΔV_O	Temperature stability			0.5		%
ΔV_O	Long term stability	1000 hrs, $T_J = 125\text{ }^{\circ}\text{C}$		0.3		%
V_{in}	Operating input voltage	$I_O = 100\text{ mA}$			15	V
I_d	Quiescent current	$V_{in} \leq 10\text{ V}$		5	10	mA
I_O	Output current	$V_{in} = 7.5\text{ V}$, $T_J = 25\text{ }^{\circ}\text{C}$	800	950	1300	mA
eN	Output noise voltage	$B = 10\text{ Hz}$ to 10 kHz , $T_J = 25\text{ }^{\circ}\text{C}$		100		μV
SVR	Supply voltage rejection	$I_O = 40\text{ mA}$, $f = 120\text{ Hz}$, $T_J = 25\text{ }^{\circ}\text{C}$ $V_{in} = 5.5\text{ V}$, $V_{ripple} = 1\text{ V}_{PP}$	60	75		dB
V_d	Dropout voltage	$I_O = 100\text{ mA}$		1	1.1	V
		$I_O = 500\text{ mA}$		1.05	1.15	
		$I_O = 800\text{ mA}$		1.10	1.2	
	Thermal regulation	$T_a = 25\text{ }^{\circ}\text{C}$, 30 ms Pulse		0.01	0.1	%/W



OPA2604

www.burr-brown.com/databook/OPA2604.html

Dual FET-Input, Low Distortion OPERATIONAL AMPLIFIER

FEATURES

- LOW DISTORTION: 0.0003% at 1kHz
- LOW NOISE: $10\text{nV}/\sqrt{\text{Hz}}$
- HIGH SLEW RATE: $25\text{V}/\mu\text{s}$
- WIDE GAIN-BANDWIDTH: 20MHz
- UNITY-GAIN STABLE
- WIDE SUPPLY RANGE: $V_S = \pm 4.5$ to $\pm 24\text{V}$
- DRIVES 600Ω LOADS

APPLICATIONS

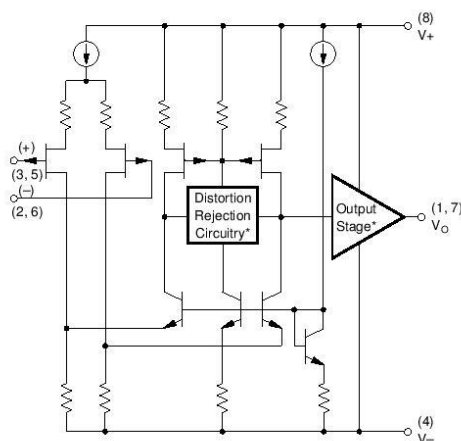
- PROFESSIONAL AUDIO EQUIPMENT
- PCM DAC I/V CONVERTER
- SPECTRAL ANALYSIS EQUIPMENT
- ACTIVE FILTERS
- TRANSDUCER AMPLIFIER
- DATA ACQUISITION

DESCRIPTION

The OPA2604 is a dual, FET-input operational amplifier designed for enhanced AC performance. Very low distortion, low noise and wide bandwidth provide superior performance in high quality audio and other applications requiring excellent dynamic performance.

New circuit techniques and special laser trimming of dynamic circuit performance yield very low harmonic distortion. The result is an op amp with exceptional sound quality. The low-noise FET input of the OPA2604 provides wide dynamic range, even with high source impedance. Offset voltage is laser-trimmed to minimize the need for interstage coupling capacitors.

The OPA2604 is available in 8-pin plastic mini-DIP and SO-8 surface-mount packages, specified for the -25°C to $+85^\circ\text{C}$ temperature range.



* Patents Granted:
#5053718, 5019789

International Airport Industrial Park • Mailing Address: PO Box 11400, Tucson, AZ 85734 • Street Address: 6730 S. Tucson Blvd., Tucson, AZ 85706 • Tel: (520) 746-1111 • Twx: 910-952-1111
Internet: <http://www.burr-brown.com/> • FAXLine: (800) 548-6133 (US/Canada Only) • Cable: BBRCORP • Telex: 066-6491 • FAX: (520) 889-1510 • Immediate Product Info: (800) 548-6132

SPECIFICATIONS

ELECTRICAL

At $T_A = +25^{\circ}\text{C}$, $V_S = \pm 15\text{V}$, unless otherwise noted.

PARAMETER	CONDITION	OPA2604AP, AU			UNITS
		MIN	TYP	MAX	
OFFSET VOLTAGE Input Offset Voltage Average Drift Power Supply Rejection	$V_S = \pm 5 \text{ to } \pm 24\text{V}$	70	± 1 ± 8 80	± 5	mV $\mu\text{V}/^{\circ}\text{C}$ dB
INPUT BIAS CURRENT ⁽¹⁾ Input Bias Current Input Offset Current	$V_{CM} = 0\text{V}$ $V_{CM} = 0\text{V}$		100 ± 4		pA pA
NOISE Input Voltage Noise Noise Density: $f = 10\text{Hz}$ $f = 100\text{Hz}$ $f = 1\text{kHz}$ $f = 10\text{kHz}$ Voltage Noise, BW = 20Hz to 20kHz Input Bias Current Noise Current Noise Density, $f = 0.1\text{Hz}$ to 20kHz			25 15 11 10 1.5 6		$\text{nV}/\sqrt{\text{Hz}}$ $\text{nV}/\sqrt{\text{Hz}}$ $\text{nV}/\sqrt{\text{Hz}}$ $\text{nV}/\sqrt{\text{Hz}}$ $\mu\text{Vp-p}$ $\text{fA}/\sqrt{\text{Hz}}$
INPUT VOLTAGE RANGE Common-Mode Input Range Common-Mode Rejection	$V_{CM} = \pm 12\text{V}$	± 12 80	± 13 100		V dB
INPUT IMPEDANCE Differential Common-Mode			$10^{12} \parallel 8$ $10^{12} \parallel 10$		$\Omega \parallel \text{pF}$ $\Omega \parallel \text{pF}$
OPEN-LOOP GAIN Open-Loop Voltage Gain	$V_O = \pm 10\text{V}$, $R_L = 1\text{k}\Omega$	80	100		dB
FREQUENCY RESPONSE Gain-Bandwidth Product Slew Rate Settling Time: 0.01% 0.1% Total Harmonic Distortion + Noise (THD+N) Channel Separation	$G = 100$ 20Vp-p, $R_L = 1\text{k}\Omega$ $G = -1$, 10V Step $G = 1$, $f = 1\text{kHz}$ $V_O = 3.5\text{Vrms}$, $R_L = 1\text{k}\Omega$ $f = 1\text{kHz}$, $R_L = 1\text{k}\Omega$	15	20 25 1.5 1 0.0003 142		MHz V/ μs μs μs % dB
OUTPUT Voltage Output Current Output Short Circuit Current Output Resistance, Open-Loop	$R_L = 600\Omega$ $V_O = \pm 12\text{V}$	± 11	± 12 ± 35 ± 40 25		V mA mA Ω
POWER SUPPLY Specified Operating Voltage Operating Voltage Range Current, Total Both Amplifiers	$I_O = 0$	± 4.5	± 15 ± 10.5	± 24 ± 12	V V mA
TEMPERATURE RANGE Specification Storage Thermal Resistance ⁽²⁾ , θ_{JA}		-25 -40		+85 +125	$^{\circ}\text{C}$ $^{\circ}\text{C}$ $^{\circ}\text{C/W}$

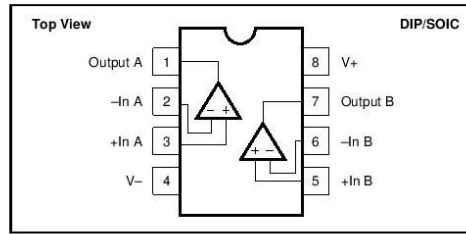
NOTES: (1) Typical performance, measured fully warmed-up. (2) Soldered to circuit board—see text.

The information provided herein is believed to be reliable; however, BURR-BROWN assumes no responsibility for inaccuracies or omissions. BURR-BROWN assumes no responsibility for the use of this information, and all use of such information shall be entirely at the user's own risk. Prices and specifications are subject to change without notice. No patent rights or licenses to any of the circuits described herein are implied or granted to any third party. BURR-BROWN does not authorize or warrant any BURR-BROWN product for use in life support devices and/or systems.



OPA2604

PIN CONFIGURATION



ELECTROSTATIC DISCHARGE SENSITIVITY

Any integrated circuit can be damaged by ESD. Burr-Brown recommends that all integrated circuits be handled with appropriate precautions. Failure to observe proper handling and installation procedures can cause damage.

ESD damage can range from subtle performance degradation to complete device failure. Precision integrated circuits may be more susceptible to damage because very small parametric changes could cause the device not to meet published specifications.

ABSOLUTE MAXIMUM RATINGS⁽¹⁾

Power Supply Voltage	±25V
Input Voltage	(V-) -1V to (V+) +1V
Output Short Circuit to Ground	Continuous
Operating Temperature	-40°C to +100°C
Storage Temperature	-40°C to +125°C
Junction Temperature	+150°C
Lead Temperature (soldering, 10s) AP	+300°C
Lead Temperature (soldering, 3s) AU	+260°C

NOTE: (1) Stresses above these ratings may cause permanent damage.

ORDERING INFORMATION

PRODUCT	PACKAGE	TEMP. RANGE
OPA2604AP	8-Pin Plastic DIP	-25°C to +85°C
OPA2604AU	SO-8 Surface-Mount	-25°C to +85°C

PACKAGING INFORMATION

PRODUCT	PACKAGE	PACKAGE DRAWING NUMBER ⁽¹⁾
OPA2604AP	8-Pin Plastic DIP	006
OPA2604AU	SO-8 Surface-Mount	182

NOTE: (1) For detailed drawing and dimension table, please see end of data sheet, or Appendix C of Burr-Brown IC Data Book.



USBLC6-2

Very low capacitance ESD protection

Features

- 2 data-line protection
- Protects V_{BUS}
- Very low capacitance: 3.5 pF max.
- Very low leakage current: 150 nA max.
- SOT-666 and SOT23-6L packages
- RoHS compliant

Benefits

- Very low capacitance between lines to GND for optimized data integrity and speed
- Low PCB space consumption: 2.9 mm² max for SOT-666 and 9 mm² max for SOT23-6L
- Enhanced ESD protection: IEC 61000-4-2 level 4 compliance guaranteed at device level, hence greater immunity at system level
- ESD protection of V_{BUS}
- High reliability offered by monolithic integration
- Low leakage current for longer operation of battery powered devices
- Fast response time
- Consistent D+ / D- signal balance:
 - Very low capacitance matching tolerance
 - I/O to GND = 0.015 pF
 - Compliant with USB 2.0 requirements

Complies with the following standards:

- IEC 61000-4-2 level 4:
 - 15 kV (air discharge)
 - 8 kV (contact discharge)

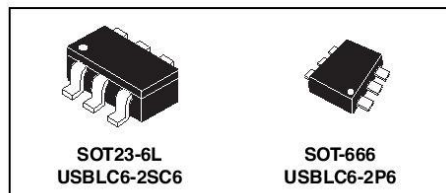
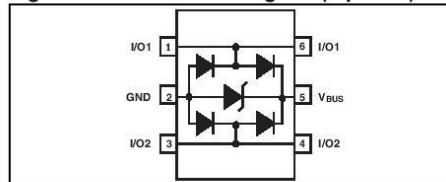


Figure 1. Functional diagram (top view)



Applications

- USB 2.0 ports up to 480 Mb/s (high speed)
- Compatible with USB 1.1 low and full speed
- Ethernet port: 10/100 Mb/s
- SIM card protection
- Video line protection
- Portable electronics

Description

The USBLC6-2SC6 and USBLC6-2P6 are monolithic application specific devices dedicated to ESD protection of high speed interfaces, such as USB 2.0, Ethernet links and video lines.

The very low line capacitance secures a high level of signal integrity without compromising in protecting sensitive chips against the most stringently characterized ESD strikes.

1 Characteristics

Table 1. Absolute ratings

Symbol	Parameter		Value	Unit
V_{PP}	Peak pulse voltage	IEC 61000-4-2 air discharge	15	kV
		IEC 61000-4-2 contact discharge	15	
		MIL STD883G-Method 3015-7	25	
T_{stg}	Storage temperature range		-55 to +150	°C
T_j	Operating junction temperature range		-40 to +125	°C
T_L	Lead solder temperature (10 seconds duration)		260	°C

Table 2. Electrical characteristics ($T_{amb} = 25\text{ °C}$)

Symbol	Parameter	Test conditions	Value			Unit
			Min.	Typ.	Max.	
I_{RM}	Leakage current	$V_{RM} = 5.25\text{ V}$		10	150	nA
V_{BR}	Breakdown voltage between V_{BUS} and GND	$I_R = 1\text{ mA}$	6			V
V_F	Forward voltage	$I_F = 10\text{ mA}$			1.1	V
V_{CL}	Clamping voltage	$I_{PP} = 1\text{ A}$, 8/20 μs Any I/O pin to GND			12	V
		$I_{PP} = 5\text{ A}$, 8/20 μs Any I/O pin to GND			17	V
$C_{i/o-GND}$	Capacitance between I/O and GND	$V_R = 1.65\text{ V}$		2.5	3.5	pF
$\Delta C_{i/o-GND}$				0.015		
$C_{i/o-i/o}$	Capacitance between I/O	$V_R = 1.65\text{ V}$		1.2	1.7	pF
$\Delta C_{i/o-i/o}$				0.04		

Future Technology Devices International Ltd.

FT232R USB UART IC



The FT232R is a USB to serial UART interface with the following advanced features:

- Single chip USB to asynchronous serial data transfer interface.
- Entire USB protocol handled on the chip. No USB specific firmware programming required.
- Fully integrated 1024 bit EEPROM storing device descriptors and CBUS I/O configuration.
- Fully integrated USB termination resistors.
- Fully integrated clock generation with no external crystal required plus optional clock output selection enabling a glue-less interface to external MCU or FPGA.
- Data transfer rates from 300 baud to 3 Mbaud (RS422, RS485, RS232) at TTL levels.
- 128 byte receive buffer and 256 byte transmit buffer utilising buffer smoothing technology to allow for high data throughput.
- FTDI's royalty-free Virtual Com Port (VCP) and Direct (D2XX) drivers eliminate the requirement for USB driver development in most cases.
- Unique USB FTDIChip-ID™ feature.
- Configurable CBUS I/O pins.
- Transmit and receive LED drive signals.
- UART interface support for 7 or 8 data bits, 1 or 2 stop bits and odd / even / mark / space / no parity
- FIFO receive and transmit buffers for high data throughput.
- Synchronous and asynchronous bit bang interface options with RD# and WR# strobes.
- Device supplied pre-programmed with unique USB serial number.
- Supports bus powered, self powered and high-power bus powered USB configurations.
- Integrated +3.3V level converter for USB I/O.
- Integrated level converter on UART and CBUS for interfacing to between +1.8V and +5V logic.
- True 5V/3.3V/2.8V/1.8V CMOS drive output and TTL input.
- Configurable I/O pin output drive strength.
- Integrated power-on-reset circuit.
- Fully integrated AVCC supply filtering - no external filtering required.
- UART signal inversion option.
- +3.3V (using external oscillator) to +5.25V (internal oscillator) Single Supply Operation.
- Low operating and USB suspend current.
- Low USB bandwidth consumption.
- UHCI/OHCI/EHCI host controller compatible.
- USB 2.0 Full Speed compatible.
- -40°C to 85°C extended operating temperature range.
- Available in compact Pb-free 28 Pin SSOP and QFN-32 packages (both RoHS compliant).

Neither the whole nor any part of the information contained in, or the product described in this manual, may be adapted or reproduced in any material or electronic form without the prior written consent of the copyright holder. This product and its documentation are supplied on an as-is basis and no warranty as to their suitability for any particular purpose is either made or implied. Future Technology Devices International Ltd will not accept any claim for damages howsoever arising as a result of use or failure of this product. Your statutory rights are not affected. This product or any variant of it is not intended for use in any medical appliance, device or system in which the failure of the product might reasonably be expected to result in personal injury. This document provides preliminary information that may be subject to change without notice. No freedom to use patents or other intellectual property rights is implied by the publication of this document. Future Technology Devices International Ltd, Unit 1, 2 Seaward Place, Centurion Business Park, Glasgow G41 1HH United Kingdom. Scotland Registered Company Number: SC136640

3 Device Pin Out and Signal Description

3.1 28-LD SSOP Package

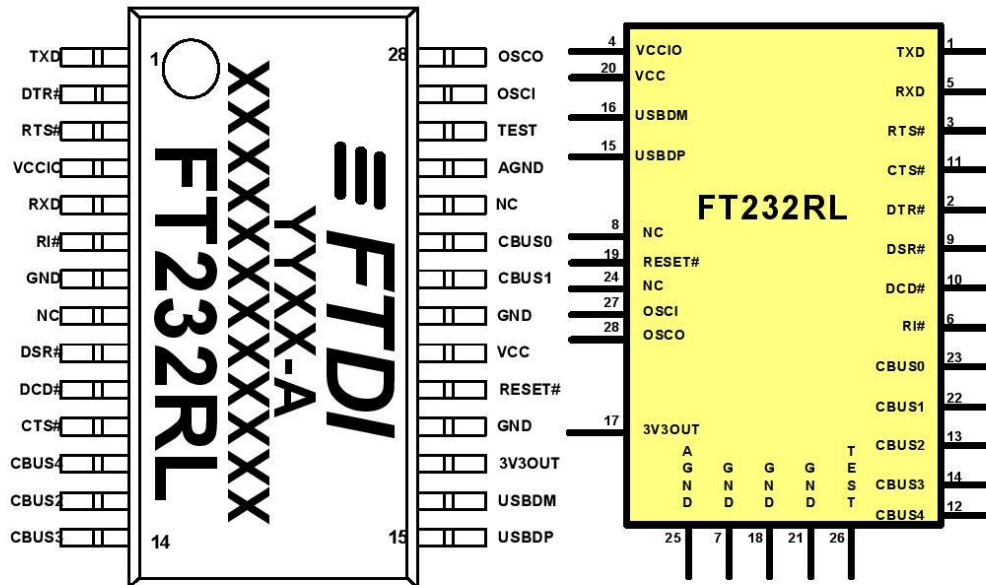


Figure 3.1 SSOP Package Pin Out and Schematic Symbol

3.2 SSOP Package Pin Out Description

Note: The convention used throughout this document for active low signals is the signal name followed by a #

Pin No.	Name	Type	Description
15	USBDP	I/O	USB Data Signal Plus, incorporating internal series resistor and 1.5kΩ pull up resistor to 3.3V.
16	USBDM	I/O	USB Data Signal Minus, incorporating internal series resistor.

Table 3.1 USB Interface Group

Pin No.	Name	Type	Description
4	VCCIO	PWR	+1.8V to +5.25V supply to the UART Interface and CBUS group pins (1...3, 5, 6, 9...14, 22, 23). In USB bus powered designs connect this pin to 3V3OUT pin to drive out at +3.3V levels, or connect to VCC to drive out at 5V CMOS level. This pin can also be supplied with an external +1.8V to +2.8V supply in order to drive outputs at lower levels. It should be noted that in this case this supply should originate from the same source as the supply to VCC. This means that in bus powered designs a regulator which is supplied by the +5V on the USB bus should be used.
7, 18, 21	GND	PWR	Device ground supply pins



Pin No.	Name	Type	Description
17	3V3OUT	Output	+3.3V output from integrated LDO regulator. This pin should be decoupled to ground using a 100nF capacitor. The main use of this pin is to provide the internal +3.3V supply to the USB transceiver cell and the internal 1.5k Ω pull up resistor on USBDP. Up to 50mA can be drawn from this pin to power external logic if required. This pin can also be used to supply the VCCIO pin.
20	VCC	PWR	+3.3V to +5.25V supply to the device core. (see Note 1)
25	AGND	PWR	Device analogue ground supply for internal clock multiplier

Table 3.2 Power and Ground Group

Pin No.	Name	Type	Description
8, 24	NC	NC	No internal connection
19	RESET#	Input	Active low reset pin. This can be used by an external device to reset the FT232R. If not required can be left unconnected, or pulled up to VCC.
26	TEST	Input	Puts the device into IC test mode. Must be tied to GND for normal operation, otherwise the device will appear to fail.
27	OSCI	Input	Input 12MHz Oscillator Cell. Optional - Can be left unconnected for normal operation. (see Note 2)
28	OSCO	Output	Output from 12MHZ Oscillator Cell. Optional - Can be left unconnected for normal operation if internal Oscillator is used. (see Note 2)

Table 3.3 Miscellaneous Signal Group

Pin No.	Name	Type	Description
1	TXD	Output	Transmit Asynchronous Data Output.
2	DTR#	Output	Data Terminal Ready Control Output / Handshake Signal.
3	RTS#	Output	Request to Send Control Output / Handshake Signal.
5	RXD	Input	Receiving Asynchronous Data Input.
6	RI#	Input	Ring Indicator Control Input. When remote wake up is enabled in the internal EEPROM taking RI# low (20ms active low pulse) can be used to resume the PC USB host controller from suspend.
9	DSR#	Input	Data Set Ready Control Input / Handshake Signal.
10	DCD#	Input	Data Carrier Detect Control Input.
11	CTS#	Input	Clear To Send Control Input / Handshake Signal.
12	CBUS4	I/O	Configurable CBUS output only Pin. Function of this pin is configured in the device internal EEPROM. Factory default configuration is SLEEP#. See CBUS Signal Options, Table 3.9.
13	CBUS2	I/O	Configurable CBUS I/O Pin. Function of this pin is configured in the device internal EEPROM. Factory default configuration is TXDEN. See CBUS Signal Options, Table 3.9.



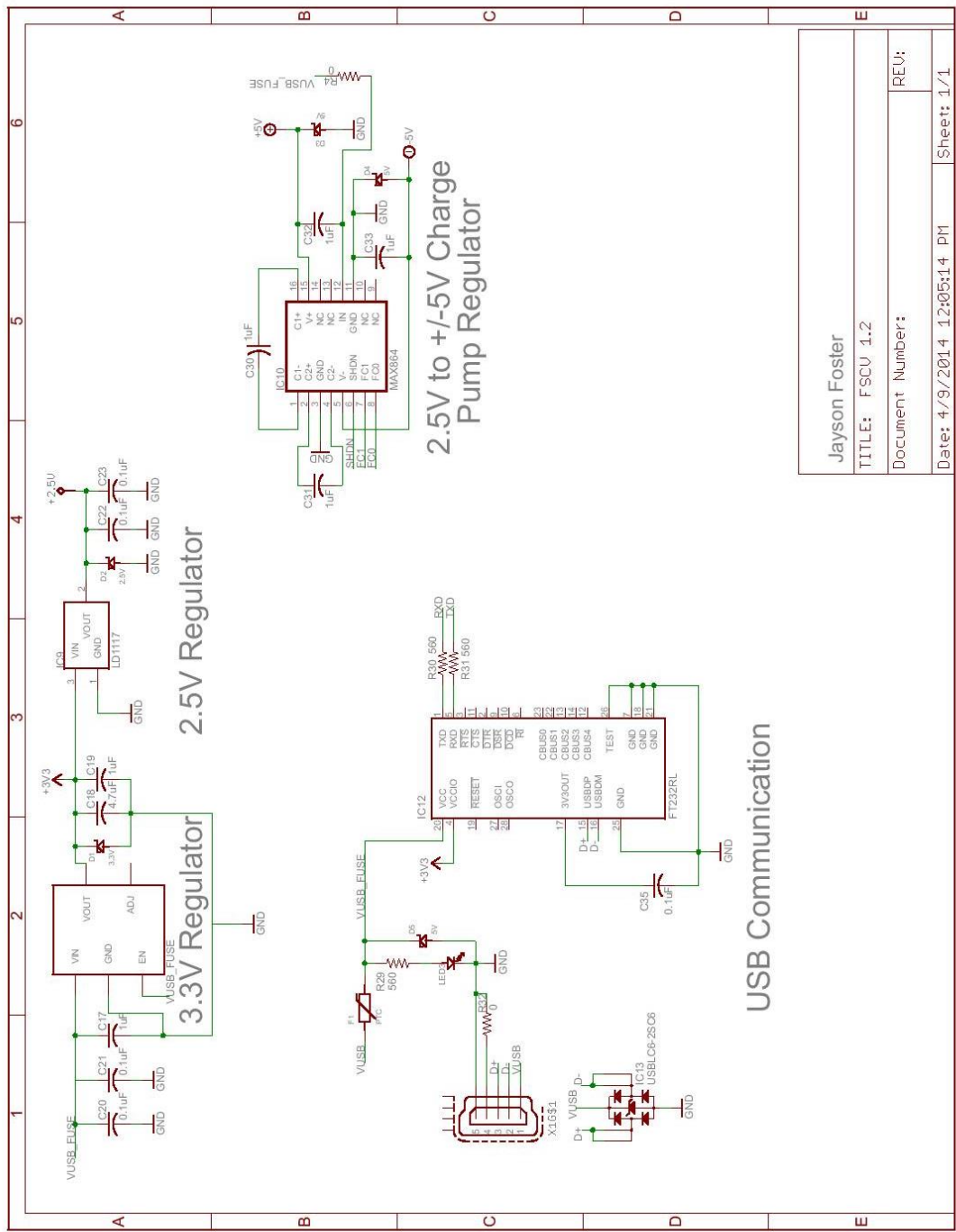
Pin No.	Name	Type	Description
14	CBUS3	I/O	Configurable CBUS I/O Pin. Function of this pin is configured in the device internal EEPROM. Factory default configuration is PWREN#. See CBUS Signal Options, Table 3.9. PWREN# should be used with a 10k Ω resistor pull up.
22	CBUS1	I/O	Configurable CBUS I/O Pin. Function of this pin is configured in the device internal EEPROM. Factory default configuration is RXLED#. See CBUS Signal Options, Table 3.9.
23	CBUS0	I/O	Configurable CBUS I/O Pin. Function of this pin is configured in the device internal EEPROM. Factory default configuration is TXLED#. See CBUS Signal Options, Table 3.9.

Table 3.4 UART Interface and CUSB Group (see note 3)

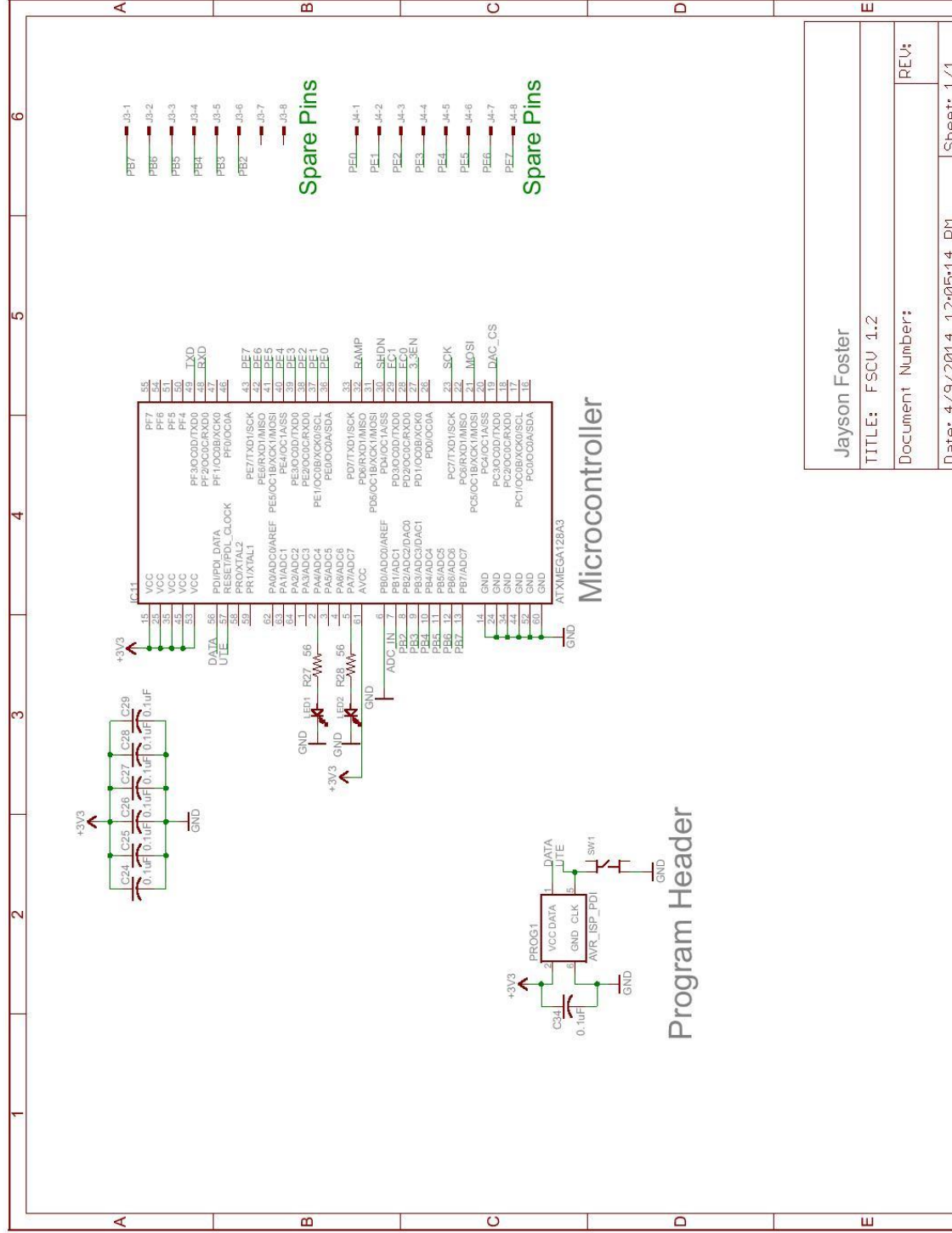
Notes:

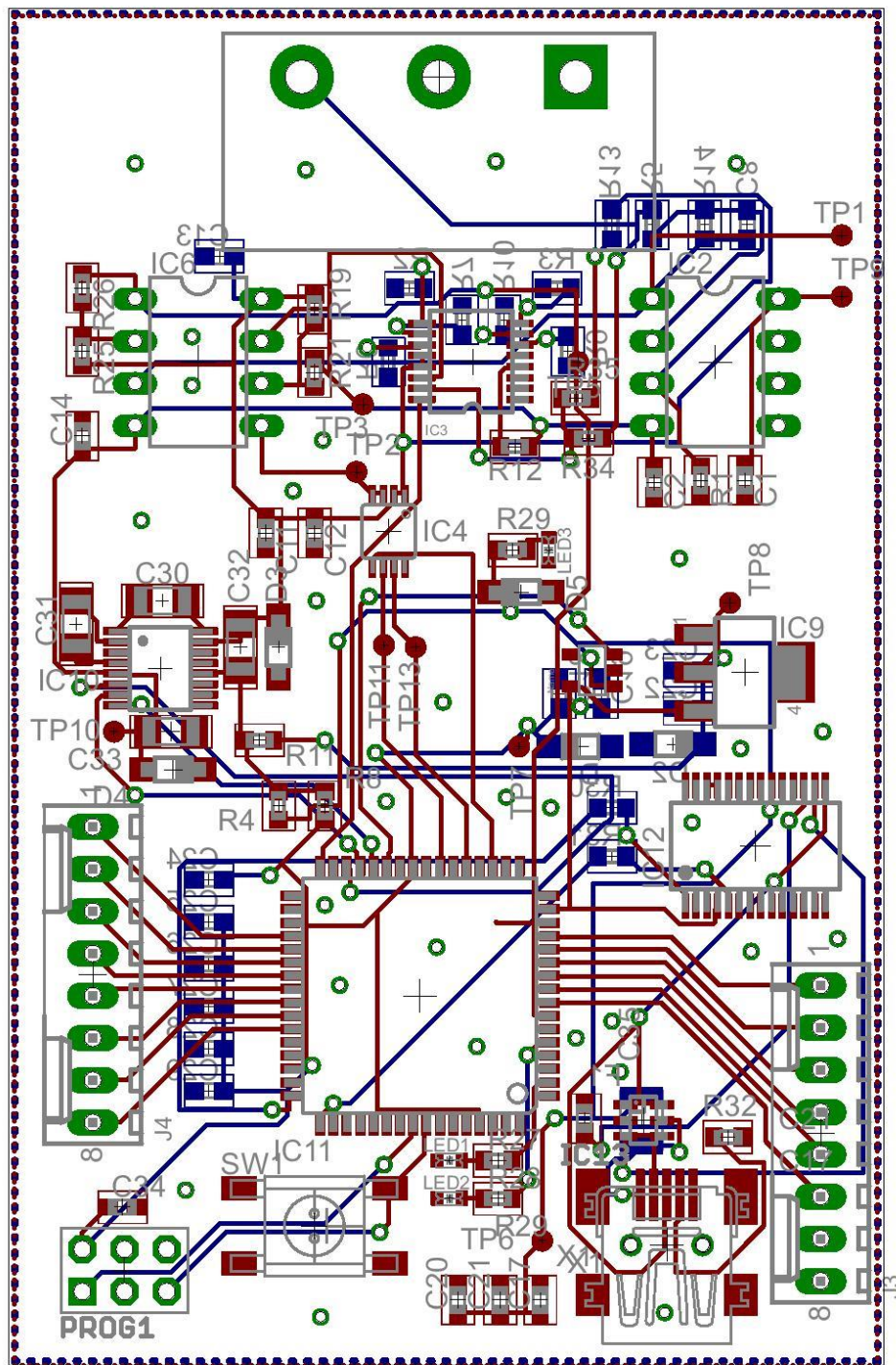
1. The minimum operating voltage VCC must be +4.0V (could use VBUS=+5V) when using the internal clock generator. Operation at +3.3V is possible using an external crystal oscillator.
2. For details on how to use an external crystal, ceramic resonator, or oscillator with the FT232R, please refer Section 7.6
3. When used in Input Mode, the input pins are pulled to VCCIO via internal 200k Ω resistors. These pins can be programmed to gently pull low during USB suspend (PWREN# = "1") by setting an option in the internal EEPROM.

Appendix II – Schematic



Jayson Foster	
TITLE: FSCU 1.2	
Document Number:	REV:
Date: 4/9/2014 12:05:14 PM	Sheet: 1/1





Appendix III – Matlab Code

```
% *****
% serial_plot.m
% Portable Fast-Scan Cyclic Voltammetry Project
% Jayson Foster
% 4/9/2014
%
% This program takes data in from the USB port of a computer hooked up to
% the portable FSCV device and converts it to usable current readings for
% display.
% *****

clc;
clear all;
close all;

s = serial('COM7'); %assigns the object s to serial port

% NOTE: for error "Open failed: Port: COM7 is not available. Available ports: COM6, COM7"
% use delete(instrfind) command to close port and make it available for
% function use

set(s, 'InputBufferSize', 2048); %number of bytes in inout buffer formally 256
set(s, 'FlowControl', 'none');
set(s, 'BaudRate', 9600);
set(s, 'Parity', 'none');
set(s, 'DataBits', 8);
set(s, 'StopBit', 1);
set(s, 'Timeout', 10);
%clc;

disp(get(s, 'Name'));
prop(1)=(get(s, 'BaudRate'));
prop(2)=(get(s, 'DataBits'));
prop(3)=(get(s, 'StopBit'));
prop(4)=(get(s, 'InputBufferSize'));

disp(['Port Setup Done!!', num2str(prop)]);

u = 1;
```

```

CompleteData = 0;
UnsignedPortion = 0;

negflag = 0;
posflag = 0;
BadData = 0;

voltage = 0;

fopen(s);      %opens the serial port
t=1;
disp('Running');
x=0;
%rawdata = zeros (500,1); % Preallocating buffer

while(s.BytesAvailable < 1712) %2048
    % Do nothing
    if(s.BytesAvailable ~= 0);
        display(s.BytesAvailable);
    end
end

rawdata = fread(s,1712,'uint8');

% CompleteData = (bitshift(uint16(rawdata(t)),8) + uint16(rawdata(t+1)));
% disp(['CompleteData =',num2str(CompleteData),' sign =', num2str(bitshift(uint16(CompleteData(u)),-
12)),]);

while(t<1712)
    CompleteData(u) = (bitshift(uint16(rawdata(t)),8) + uint16(rawdata(t+1)));

    % If data is 1111 1xxx xxxx xxxx then it is negative
    % If data is 0000 0xxx xxxx xxxx then it is positive
    if(bitshift(uint16(CompleteData(u)),-11) == 31)
        negflag = 1;
        disp('Neg Value');
    elseif(bitshift(uint16(CompleteData(u)),-11) == 0)
        posflag = 1;
        disp('Pos Value');
    else

```

```

        BadData = 1;
        disp('Bad Data');
    end

    UnsignedPortion = bitand(uint16(CompleteData(u)),uint16(4095));%2047));

    if(negflag == 1)
        voltage(u) = twos2dec(dec2bin(UnsignedPortion))*(2.06/2048);
        if(voltage(u) < -5)
            BadData = 1;
        end
    elseif(posflag == 1)
        voltage(u) = bin2dec(dec2bin(UnsignedPortion))*(2.06/2048);
        if(voltage(u) > 5)
            BadData = 1;
        end
    end
end

if(BadData == 1)
    t = t + 1;
    disp('BadData triggered');
else
    x(u) = voltage(u);

    disp([num2str(t),'th iteration = ',num2str(voltage(u)), ' 12-bit value = ',num2str(UnsignedPortion),'
Byte 1 = ',num2str(rawdata(t)),' Byte 2 = ',num2str(rawdata(t+1))]);
    hold on;

    u = u + 1;

    t=t+2;
end

BadData = 0;
negflag = 0;
posflag = 0;

end

%smooth(x);
cleandata=x(x~=0);

```

```
plot(cleandata, '-x');  
axis auto;  
grid on;  
  
fclose(s); %close the serial port
```

```

function x = twos2dec(t)

% TWOS2DEC Convert binary string two's complement to decimal integer.
%
% Usage: X = TWOS2DEC(T)
%
% Converts the two's complement representation as a string given by T to
% decimal integers X. T can be a character array or cell string. Input
% multiple numbers into T along the rows, and the output will be as a
% column vector. Similarly to BIN2DEC, leading spaces in T are sign
% extended (so treated as either 0 or 1 depending on the first non space
% character), and embedded and trailing spaces are removed.
%
% Example:
% >> twos2dec(['010 111'; ' 010111'; '101011 '; ' 10  1'])
%
%    ans =
%
%        23
%        23
%       -21
%        -3
%
% Inputs:
% -T: string two's complement numbers to convert to decimal integers.
%
% Outputs:
% -X: decimal representation of T.
%
% See also: DEC2TWOS, FIX2DEC, DEC2FIX, BIN2DEC, HEX2DEC, BASE2DEC.

%Error check
narginchk(1, 1);
if iscellstr(t)
    t = char(t);
end

% Convert to numbers.
x = bin2dec(t);

% Get the number of bits as the number of 0's and 1's in each row.

```

```

nbits = sum(t == '0' | t == '1', 2);

% Case for negative numbers.
xneg = log2(x) >= nbits - 1;
% xneg = bitshift(x, -(nbits - 1)) == 1;
if any(xneg)
    x(xneg) = -( bitcmp(x(xneg), nbits(xneg)) + 1 );
end

```

function two2dec.m
Copyright (c) 2012, Drew Compston
All rights reserved.

Redistribution and use in source and binary forms, with or without
modification, are permitted provided that the following conditions are
met:

- * Redistributions of source code must retain the above copyright
notice, this list of conditions and the following disclaimer.
- * Redistributions in binary form must reproduce the above copyright
notice, this list of conditions and the following disclaimer in
the documentation and/or other materials provided with the distribution

THIS SOFTWARE IS PROVIDED BY THE COPYRIGHT HOLDERS AND CONTRIBUTORS "AS IS"
AND ANY EXPRESS OR IMPLIED WARRANTIES, INCLUDING, BUT NOT LIMITED TO, THE
IMPLIED WARRANTIES OF MERCHANTABILITY AND FITNESS FOR A PARTICULAR PURPOSE
ARE DISCLAIMED. IN NO EVENT SHALL THE COPYRIGHT OWNER OR CONTRIBUTORS BE
LIABLE FOR ANY DIRECT, INDIRECT, INCIDENTAL, SPECIAL, EXEMPLARY, OR
CONSEQUENTIAL DAMAGES (INCLUDING, BUT NOT LIMITED TO, PROCUREMENT OF
SUBSTITUTE GOODS OR SERVICES; LOSS OF USE, DATA, OR PROFITS; OR BUSINESS
INTERRUPTION) HOWEVER CAUSED AND ON ANY THEORY OF LIABILITY, WHETHER IN
CONTRACT, STRICT LIABILITY, OR TORT (INCLUDING NEGLIGENCE OR OTHERWISE)
ARISING IN ANY WAY OUT OF THE USE OF THIS SOFTWARE, EVEN IF ADVISED OF THE
POSSIBILITY OF SUCH DAMAGE.

Appendix IV – DAC Microcontroller Code

```
/*
 * gvsuFSCV.c
 *
 * Created: 1/11/2012 3:09:36 PM
 * Author: grant
 *
 * Modified and updated: 4/9/2014
 *             Jayson Foster
 *
 * Fast Scan Cyclic Voltammetry code for microcontroller handling DAC
 * This code generates the stimulus triangle waveform for FSCV
 */

#include "avr_compiler.h"
#include "clksys_driver.h"
#include "util.h"
#include <util/delay.h>
#include <avr/interrupt.h>
#include "string.h"
// #include <avr/iom128a.h>
#include <stdbool.h>
#include "spi_driver.h"
#include "dac.h"
#include "usart_driver.h"
#include "stdio.h"
#include "adc.h"
#include <stddef.h>
#include <avr/pgmspace.h>

#define lookupLength 1350 //Real value is dialed in by calibration: looking at waveform
                           through oscilloscope, same for dacBase and dacTop
#define triangleLength 70
#define DAC 1
#define ADC 0
#define dacBase 30000 // Min value: 0
#define dacTop 42000 // Max value: 65536

// USART output for data
#define USART USARTF0
#define NUM_BYTES 2048
uint8_t sendArray[NUM_BYTES];
uint8_t i;
USART_data_t USART_data;

uint16_t adc_result;
uint8_t result_flag = 0;
uint16_t pot_val = 0x0000;
uint16_t temp_result = 0x0000;
uint8_t over_sample_num = 0x00;

uint16_t ADCB_cal;

uint16_t triangleLookup[lookupLength];
int lookupIndex = 0;
```



```

char retStatus = 0;
int adc_counter = 0;

int main(void)
{
    int i;

    //Setup the 32MHz Clock
    //start 32MHz oscillator
    CLKSYS_Enable( OSC_RC32MEN_bm );
    //wait for 32MHz oscillator to stabilize
    while ( CLKSYS_IsReady( OSC_RC32MRDY_bm ) == 0 );
    //set clock as internal 32MHz RC oscillator
    CLKSYS_Main_ClockSource_Select( CLK_SCLKSEL_RC32M_gc );

    // Initialize the Status LEDs
    initStatusLED();
    initHardware();

    for(i = 0; i <= lookupLength;i++){
        triangleLookup[i]=dacBase;
    }

    // fill the triangle wave lookup
    for(i = 1; i < triangleLength*2;i++){
        // ramp up
        if( i <= (triangleLength)){
            triangleLookup[i] = triangleLookup[i-1] + ((dacTop-
dacBase)/(triangleLength));
        }
        // ramp down
        if(i > (triangleLength)){
            triangleLookup[i] = triangleLookup[i-1] - ((dacTop-
dacBase)/(triangleLength));
        }
    }

    initDebugUSART();

    // Enable all interrupt levels
    // Load Int vectors to application section of flash
    // Set interrupt priority to Static (lower address = higher priority)
    PMIC_CTRL = PMIC_HILVLEN_bm | PMIC_MEDLVLEN_bm | PMIC_LOLVLEN_bm; //0x07

    /* Enable global interrupts. */
    sei();

    SPI_MasterInit(&spiMasterC,
                    &SPIC,
                    &PORTC,
                    false,
                    SPI_MODE_1_gc,
                    SPI_INTLVL_OFF_gc,
                    false, //false
                    SPI_PRESCALER_DIV64_gc); //SPI_PRESCALER_DIV128_gc - 64
gives 500kHz to match ADC clock

```

```

        lookupIndex = 0;
while(1)
{
    // If else statement to signal the other board to record the triangle wave
    // the +/- 25 is so that there is some resting potential captured along
with the triangle waveform
    if(lookupIndex <= (triangleLength*2)+25 || lookupIndex >= lookupLength-25){
        PORTE.OUTSET = PIN1_bm;
        statusLED(1,1);
    }
    else{
        PORTE.OUTCLR = PIN1_bm;
        statusLED(0,0);
    }

    /* DAC Triangle Wave */
    retStatus = setDAC1(triangleLookup[lookupIndex++]);
    if(lookupIndex >= lookupLength){
        lookupIndex = 0;
    }
}
}

```

Appendix V – ADC Microcontroller Code

```
/*
 * gvsuFSCV.c
 *
 * Created: 1/11/2012 3:09:36 PM
 * Author: grant
 *
 * Modified and updated: 4/9/2014
 *          Jayson Foster
 *
 * Fast Scan Cyclic Voltammetry code for microcontroller handling ADC
 *          This code records the resultant current from the triangle stimulus waveform
 */

#include "avr_compiler.h"
#include "clksys_driver.h"
#include "util.h"
#include <util/delay.h>
#include <avr/interrupt.h>
#include "string.h"
// #include <avr/iom128a.h>
#include <stdbool.h>
#include "spi_driver.h"
#include "dac.h"
#include "usart_driver.h"
#include "stdio.h"
#include "adc.h"
#include <stddef.h>
#include <avr/pgmspace.h>

#define DAC 0
#define ADC 1

#define USART USARTF0
#define NUM_BYTES 2048
uint8_t sendArray[NUM_BYTES];
uint8_t i;
USART_data_t USART_data;

uint16_t adc_result;
uint16_t pot_val = 0x0000;
uint16_t temp_result = 0x0000;
uint8_t over_sample_num = 0x00;

uint16_t ADCB_cal;

int lookupIndex = 0;
int adc_counter = 0;

// Interrupt Service Routine for handling the ADC conversion complete interrupt
ISR(ADCB_CH0_vect) {

    //adc_result = ADCB.CH0.RES;
    sendArray[adc_counter] = ADCB.CH0.RES & 0xff;
```

```

        sendArray[adc_counter+1] = (ADCB.CH0.RES >> 8);
        adc_counter = adc_counter + 2;
        //sendArray[2] = 0x0D;

        // Interrupt flag is cleared upon return from ISR
    }

    // Function to read ADC Calibration from microcontroller register
    uint8_t ReadCalibrationByte( uint8_t index )
    {
        uint8_t result;

        /* Load the NVM Command register to read the calibration row. */
        NVM_CMD = NVM_CMD_READ_CALIB_ROW_gc;
        result = pgm_read_byte(index);

        /* Clean up NVM Command register. */
        NVM_CMD = NVM_CMD_NO_OPERATION_gc;

        return( result );
    }

    int main(void)
    {
        int i;

        //Setup the 32MHz Clock
        //start 32MHz oscillator
        CLKSYS_Enable( OSC_RC32MEN_bm );
        //wait for 32MHz oscillator to stabilize
        while ( CLKSYS_IsReady( OSC_RC32MRDY_bm ) == 0 );
        //set clock as internal 32MHz RC oscillator
        CLKSYS_Main_ClockSource_Select( CLK_SCLKSEL_RC32M_gc );

        // Initialize the Status LEDs
        initStatusLED();
        initHardware();
        initDebugUSART();

        // Enable all interrupt levels
        // Load Int vectors to application section of flash
        // Set interrupt priority to Static (lower address = higher priority)
        PMIC_CTRL = PMIC_HILVLEN_bm | PMIC_MEDLVLEN_bm | PMIC_LOLVLEN_bm; //0x07

        // Calibration values are stored at production time
        // Load stored bytes into the calibration registers
        // First NVM read is junk and must be thrown away
        ADCB.CALL = ReadCalibrationByte( offsetof(NVM_PROD_SIGNATURES_t, ADCBCAL0) );
        ADCB.CALH = ReadCalibrationByte( offsetof(NVM_PROD_SIGNATURES_t, ADCBCAL1) );
        ADCB.CALL = ReadCalibrationByte( offsetof(NVM_PROD_SIGNATURES_t, ADCBCAL0) );
        ADCB.CALH = ReadCalibrationByte( offsetof(NVM_PROD_SIGNATURES_t, ADCBCAL1) );

        // Place ADC channel in single-ended mode
        // Gain set to 1
        // Differential signal using internal ground (single ended) of differential using
        pin ground results in much more stable signal

```

```

ADCB.CH0.CTRL = ADC_CH_INPUTMODE0_bm; // 0x02

// Connect ADC line (PB1) to positive input
// MUXNEG bits are ignored in single-ended mode
ADCB.CH0.MUXCTRL = ADC_CH_MUXINT0_bm; // 0x08

// Apply no limit to ADC sample rate
// Put ADC in signed mode
// Disable Free-run mode (single conversion upon trigger)
// Resolution set to 12-bit, right justified (11-bit effective in signed mode)
ADCB.CTRLB = ADC_CONMODE_bm; // 0x10

// Set ADC clock to 250kHz: CPU_per/256 => 32MHz/256 = 125kHz
ADCB.PRESCALER = ADC_PRESCALER2_bm | ADC_PRESCALER1_bm;

// Set Vref to Vcc/1.6. This gives 3.3/1.6 = approx 2.06V
// With effectively 11-bit resolution, this means each LSB
// will represent approximately 1 mV.
ADCB.REFCTRL = ADC_REFSEL0_bm; // 0x10

// Not implementing Event System so ensure EVCTRL is reading zeros
ADCB.EVCTRL = 0x00;

// Ensure the ADC complete flag is cleared (by writing a '1' to it)
ADCB.INTFLAGS = ADC_CH0IF_bm; // 0x01

// Configure interrupt on conversion complete with high priority
ADCB.CH0.INTCTRL = ADC_CH_INTLVL1_bm | ADC_CH_INTLVL0_bm; // 0x03

// Enable ADC, module B
ADCB.CTRLA = ADC_ENABLE_bm; // 0x01

/* Enable global interrupts. */
sei();

SPI_MasterInit(&spiMasterC,
               &SPIC,
               &PORTC,
               false,
               SPI_MODE_1_gc,
               SPI_INTLVL_OFF_gc,
               false, //false
               SPI_PRESCALER_DIV64_gc); //SPI_PRESCALER_DIV128_gc - 64
gives 500kHz to match ADC clock

PORTE.DIRSET = PIN1_bm;
int first = 0;

lookupIndex = 0;
while(1)
{
    if(first == 0)
    {
        // Checks for input from DAC microcontroller for triangle wave flag
        // Code remains in while loop until triangle wave passes so that it
        constantly records data
    }
}

```

```

        while (PORTB.IN & PIN6_bm)
        {
            // Utilizing internal ADC
            // Setting flag to take a reading
            ADCB.CH0.CTRL |= 0x80;

            first = 1;
        }
    }

    // first flag is to make sure that the device only sends one recording
    between resets
    if(first == 1)
    {
        i=0;
        bool byteToBuffer;

        // Sending data out through USART to the USB IC for transmission to
        computer
        while (i < adc_counter) {
            byteToBuffer = USART_TxBuffer_PutByte(&USART_data,
            sendArray[i]);
                if(byteToBuffer){
                    i++;
                }
            }

            statusLEDTgl(1,1);

            first = 0;
        }
    }
}

```